

Realistic Shoulder Model with Soft Tissue Attachments

Fiona McEvilly, Kelly Miller, and Marilyn Senger



Worcester Polytechnic Institute

Major Qualifying Project

Professor Fiona Levey

April 27, 2023

This report represents the work of one or more WPI undergraduate students submitted to the faculty as evidence of completion of a degree requirement. WPI routinely publishes these reports on its site without editorial or peer review.

Abstract

The goal of this project was to modify an existing model of a human shoulder to achieve consistent abduction of the humerus from zero to 90 degrees with an anatomically accurate scapulohumeral rhythm. To inform our modifications, we researched the biomechanics of the shoulder and the material properties of muscles, tendons and ligaments. We selected synthetic soft tissue materials, their attachment methods, and motor placement for achieving accurate motion. Our model actuated each of five simulated muscles using stepper motors run by an Arduino Uno and coded such that the muscles would abduct the humerus and rotate the scapula in the accurate scapulohumeral rhythm. Our completed model abducted the humerus from zero to 41 degrees. The scapula consistently remained at rest until 20 degrees of humeral abduction, and then rotated 1 degree for each additional 1.67 degrees of humeral abduction. In the future, this model could be further developed and used for medical education or shoulder injury research.

Acknowledgements

Our team would like to thank a few people for their assistance and contributions towards our project. First, we would like to thank our advisor Fiona Levey for her support and feedback throughout the project. We would also like to thank Shu Guo for his assistance with our tensile testing. Our final thank you goes to the previous MQP team working on this project (Ella Dean, Danielle LaBlanc, Bailey Savage, and Shawna Winters) for their work on the previous iteration of the model and their guidance as we continued the project.

Table of Contents

Abstract	2
Acknowledgements	3
Table of Tables	6
Table of Figures	6
1. Introduction	9
2. Background	11
2.1 Literature Review	11
2.1.2 Tendons	15
2.1.3 Ligaments	17
2.1.4 Muscles	19
2.1.5 Tendon Attachment to Bone	23
2.1.6 Recent Developments in Soft Tissue Replication	25
2.1.7 Abduction	26
2.2. Prior Team's Model	30
2.2.1 Motor Placement	30
2.2.2 Soft Tissues Materials and Placement	32
2.2.3 Attachment Methods	33
3. Methodology	35
3.1 Building Methods	35
3.1.1 Build goals	35
3.1.2 Material Selection for Soft Tissues	36
3.1.3 Attachment Methods	42
3.1.4 Motor Location and Function	43
3.2 Testing Methods	50
3.2.1 Model Function Goals	50
3.2.2 Movement Tracking Dots	50
3.2.2 Testing Procedure	51
4. Results	53
4.1 Abducts to 90 degrees	53
4.2 Returns to 0 degrees	53
4.3 Accurate Scapulohumeral Rhythm	53
4.3.1 Back View	53
5. Discussion	58
6. Conclusions and Recommendations	60
7. Broader Impacts	62

	5
7.1 Engineering Ethics	62
7.2 Social and Global Impact	63
7.3 Environmental Impact	63
7.4 Economic Impact	63
8. Citations	64
9. Appendices	68
9.1 Anatomical Terminology	68
9.2 Planes of the Body	69
9.3 Ligament Function and Anatomy	70
9.4 Additional Materials Considered	72
9.5 Additional Attachment Methods Consider	74
9.6 Muscle Distances	75
9.7 Motor Code	77

Table of Tables

- Table 1: Mechanical Properties of the Supraspinatus Tendon
- Table 2: “Summary of Mechanical and Structural Mean Values (+/- standard deviation) of 83 shoulder joints at three different strain rates and two high rates combined” (Koh, 2004)
- Table 3: Elastic modulus (in kPa) of shoulder muscles before pitching, immediately after, and twenty-four hours after (Yamaura, 2021).
- Table 4: Elastic modulus of the upper trapezius both at rest and at 30° of abduction (Leong, 2013).
- Table 5: Elastic modulus (in kPa) of five regions of the deltoid muscle (A1, A2, M, P1, P2) at elongation lengths of 0 mm, 5 mm, 10 mm, 15 mm (Hatta, 2016).
- Table 6: Summary table of the elastic modulus of the five muscles represented in the current model (Yamaura, 2021; Leong, 2013; Hatta, 2016).
- Table 7: Scapula rotation based on humeral abduction angle (Lee et. al. 2020)
- Table 8: Variable descriptions for free body diagrams (Deane et al, 2022).
- Table 9: Tensile testing specimen dimensions.
- Table 10: Variable descriptions for free body diagram (Deane et al, 2022)
- Table 11: Anatomical Terminology
- Table 12: Planes of Body
- Table 13: Glenohumeral ligaments Function and Anatomy (Dekker, 2020).
- Table 14: Ligament function and Anatomy (Dekker, 2020).
- Table 15: Design Matrix for Weighing Material Selection Options
- Table 16: Explanation of Criteria Scoring for Materials
- Table 17: Decision Matrix for Attachment Methods
- Table 18: Explanation of Scoring for Attachments
- Table 19: Distance of Muscles and motor movement

Table of Figures

- Figure 1: Bones of the Shoulder (Shoulder Anatomy, n.d.)
- Figure 2: Ligaments of the Shoulder (Shoulder Anatomy, n.d.)
- Figure 3: Muscles of the Shoulder, Front View (Britannica, n.d.), with the muscles and bones included in our project highlighted yellow
- Figure 4: Muscles of the Shoulder, Back View (Singh, n.d.)
- Figure 5: Structure of a Tendon (Sensini & Cristofolini, 2018)
- Figure 6: A typical stress-strain curve for tendons (Sensini & Cristofolini, 2018)
- Figure 7: A typical stress-strain curve for ligaments (Sensini & Cristofolini, 2018)
- Figure 8: Structure of a muscle (Frontera, 2014)
- Figure 9: Regions of deltoid muscle referenced (Hatta, 2016).
- Figure 10: Layers of the enthesis
- Figure 11: Gradients of the entheses regions (Schwartz, 2013)
- Figure 12: Janis Tough Adhesive (blue) on a tendon model within a joint (Irving 2022)
- Figure 13: Hydrogel tendon material layer compared to real tendon attachment (Newsroom 2021).
- Figure 14: Shoulder abduction motion (Anatomy Language: Part II, 2014)
- Figure 15: Rotation of scapula
- Figure 16: Forces acting on the shoulder during elevation (Schenkman, M., & Rugo de Cartaya, V., 1987)
- Figure 17: Scapulohumeral Rotation
- Figure 18: Previous model's motor placement
- Figure 19: Free body diagram of forces on the humerus with current model placement.
- Figure 20: The drilling method used for muscle attachment points. The attachment points of the lower trapezius (left) and upper trapezius (right) are shown to illustrate this method.
- Figure 21: Eye hooks were used to achieve the proper line of action of the deltoid muscle.
- Figure 22: KT Tape used to replicate the acromioclavicular ligament capsule.
- Figure 23: Attachment points of bungee cords.
- Figure 24: Tensile testing set-up.
- Figure 25: Tensile testing specimen with 2mm thickness

Figure 26: Stress vs strain curve generated by tensile testing TPU at a speed of 50 mm/min until failure.

Figure 27: Stress vs strain curve generated by tensile testing Elastic at a speed of 50 mm/min until failure.

Figure 28: Stress vs strain curve generated by tensile testing Flexible at a speed of 50 mm/min until failure.

Figure 29: Comparisons of the TPU, flexible, and elastic materials. TPU1, F1, and E1 were subjected to tensile testing, while TPU2, F2, and E2 were not.

Figure 30: Free body diagram of forces on the humerus with new motor placement

Figure 31: (left) Diagram showing bowden cable on the model, (right) force vectors of the deltoid muscle and bowden cable on the humerus and scapula respectively

Figure 32: Bowden cable at use in the model on the supraspinatus muscle.

Figure 33: Circuit with arduino, microprocessors, and motors diagram (left) and set up (right)

Figure 34: Illustration showing location of stickers on the scapula. Left drawing shows the side view, middle drawing shows the back view, and right drawing shows the top view.

Figure 35: Illustration showing location of stickers on the humerus.

Figure 36: The videos of the abduction movement were analyzed using the “measure angle from vertical” tool in Kinovea.

Figure 37: Maximum abduction of trials one, two, and three.

Figure 38: Initial position of humerus for trial one

Figure 39: A graph portraying measured (blue) and ideal (orange) scapula rotation as a function of humeral abduction.

Figure 40: Scapula internal rotation as a function of humerus abduction. The scapula in the model rotates externally during abduction rather than internally.

Figure 41: Humerus deviation as a function of abduction.

1. Introduction

This project was a continuation of a previous Major Qualifying Project (MQP) working towards creating a shoulder model with biomechanically accurate motion (Deane et al, 2022). The previous team was able to achieve anatomically accurate placement of bones, muscles, and ligaments, using PLA, fishing line, and KT tape/bungee cords to replicate each of these materials respectively. The previous iteration consistently abducted the humerus to 60 degrees and reliably returned it to rest.

The previous team's iteration of the model had made great strides toward an anatomically accurate shoulder model with relative scapulohumeral motion, which is the coordinated motion of the scapula and humerus during abduction. Despite these great strides, there were several areas for improvement which we aimed to address. One major area of improvement was making the scapulohumeral rhythm more accurate. Ideally, the scapula should remain at rest until the humerus has reached 30 degrees of abduction, and then rotate one degree for every two degrees of humeral abduction. In the previous iteration, the scapula began rotating immediately at a consistent ratio of one degree of scapula rotation to three degrees of humeral abduction, which is within 50% of the average ratio which is 1:2. The second major area of improvement was utilizing materials that better replicated the mechanical properties of biological materials and creating more accurate attachment points on the model. In the previous iteration, the materials used to replicate soft tissues were not accurate to the material properties of the natural tissues in the human body. Additionally, the attachment points on the previous iteration were simplified compared to how attachments between muscle and bone naturally occur in the body. The goal of continuing this project was to improve upon the work of the previous team by improving soft tissue material selection, attachment points, and actuation in order to improve anatomical accuracy and achieve accurate scapulohumeral movement.

By selecting materials that better mimic the mechanical properties of biological soft tissues and improving the attachment points to better imitate the gradual transition from bone to tendon to muscle, we aimed to create a more biologically and anatomically accurate model. Additionally, by adjusting the motor placement and modifying the code for the motors we intended to improve the accuracy of the scapulohumeral rhythm and achieve a full 90 degrees of abduction.

In the long term, we anticipate that the model could incorporate more ranges of motion, such as abduction past 90 degrees, adduction, flexion, extension, and internal and external rotations. In the future, this model could be used for injury prevention research, allowing researchers to simulate common shoulder injuries and better understand how to properly prevent and repair those injuries. This model could also be used for other applications, such as medical education or testing of medical devices for the shoulder.

2. Background

2.1 Literature Review

2.1.1 Overview of Anatomy

The shoulder consists of three bones: the scapula (shoulder blade), clavicle (collarbone), and humerus (upper arm bone). The glenohumeral joint is where the humerus fits into the glenoid fossa, which is a shallow cavity in the scapula. This forms a ball-in-socket joint that allows for the shoulder's wide range of motion. Another joint of the shoulder is the acromioclavicular (AC) joint. This is where the acromion (the most superior point on the scapula) meets with the clavicle. The final joint in the shoulder is the sternoclavicular (SC) joint, which is where the clavicle bone meets the sternum (breast bone). These shoulder bones can be seen in figure 1 below (*Shoulder Anatomy*, n.d.)

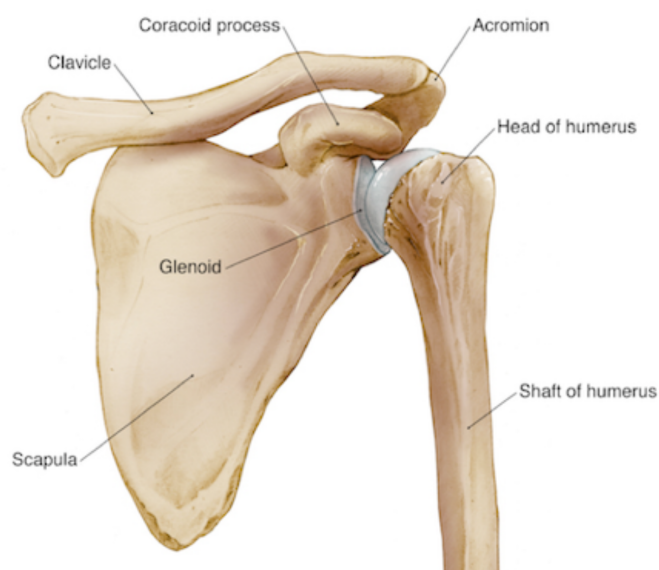


Figure 1: Bones of the Shoulder (Shoulder Anatomy, n.d.)

Within the glenohumeral joint are the glenohumeral ligaments. These ligaments are important for providing support to the joint and keeping the humerus in place while also allowing for proper movement of the shoulder. The glenoid labrum is another important structure of the glenohumeral joint. The glenoid labrum surrounds the glenoid and provides a secure location for the humeral head to fit. Other ligaments in the shoulder that are important for stabilization include the coracoclavicular ligaments, the acromioclavicular ligament, the

coracoacromial ligament, and the coraco-humeral ligament (Shoulder Anatomy, n.d.). These structures are displayed in figure 2 below. Additionally, more detailed information about these ligaments is given in Appendix A.

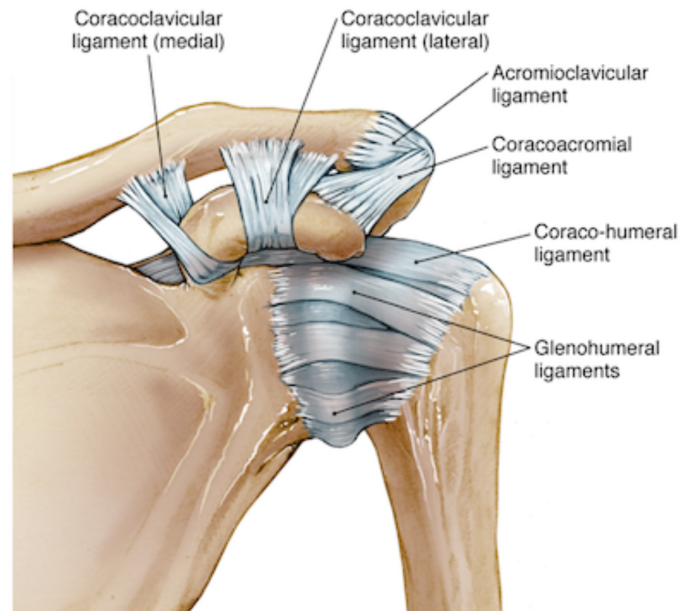
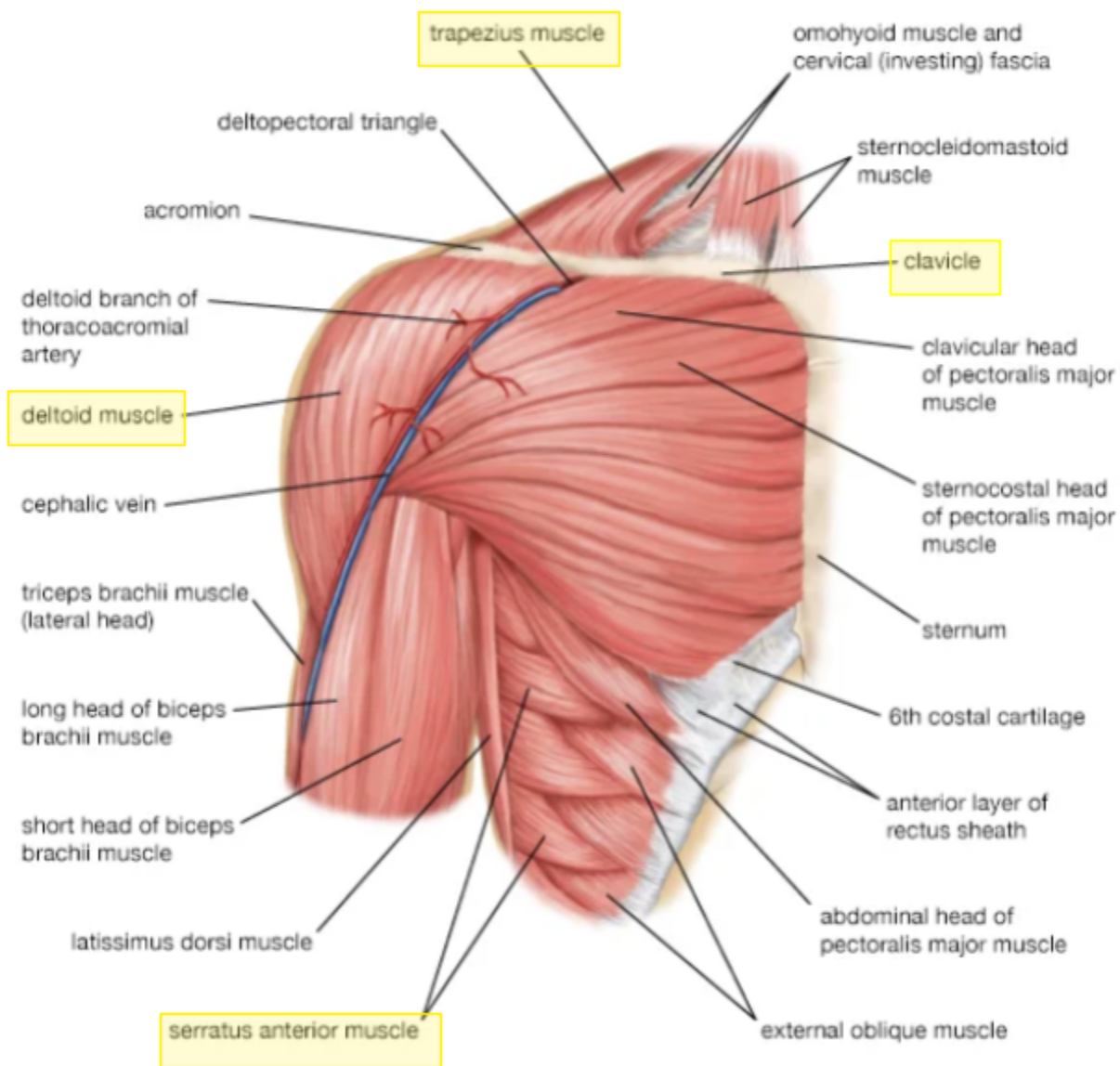


Figure 2: Ligaments of the Shoulder (Shoulder Anatomy, n.d.)

The muscles and tendons of the shoulder are also important for providing stabilization as well as movement to the shoulder joints. The tendons of the subscapularis, supraspinatus, infraspinatus, and teres minor form what is called the rotator cuff. The rotator cuff is a group of tendons that form a “cuff” around the shoulder. Rotator cuffs are a very common site of injury and overuse in the shoulder due to their location and role in shoulder movement (*Shoulder Anatomy*, n.d.). Apart from the rotator cuff muscles, other muscles of the shoulder include the deltoid, teres major, trapezius, latissimus dorsi, levator scapulae, and rhomboid muscles (Singh, n.d.). The figures below show these shoulder muscles.



© Encyclopædia Britannica, Inc.

Figure 3: Muscles of the Shoulder, Front View (Britannica, n.d.), with the muscles and bones included in our project highlighted yellow

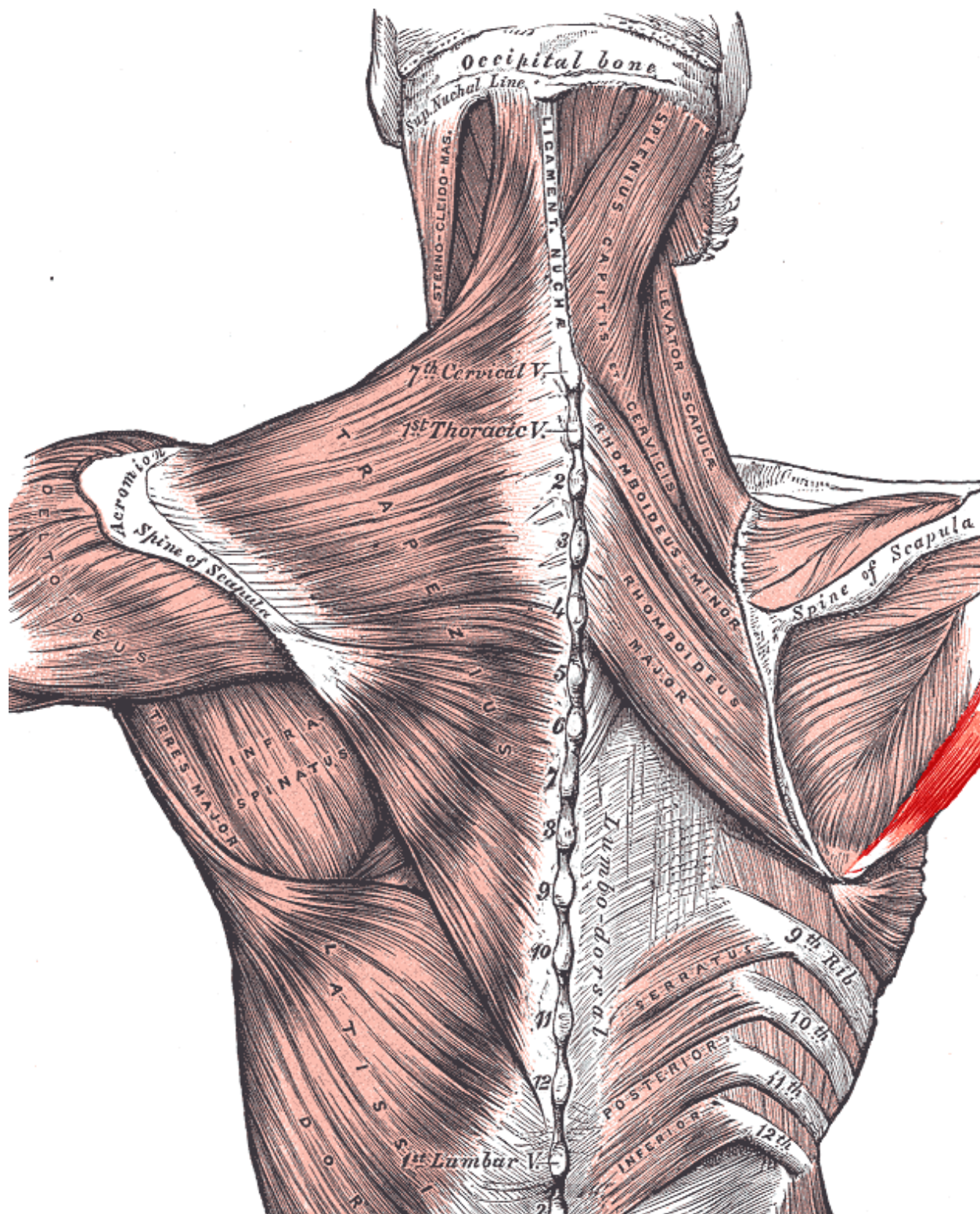


Figure 4: Muscles of the Shoulder, Back View (Singh, n.d.)

2.1.2 Tendons

Tendons are the soft tissues that connect muscles to bones. They transmit forces from the muscles to the joints and provide stabilization. About 70-80% of the dry weight within tendons is collagen. This collagen is arranged within the tendon in a hierarchical structure. On a microscopic level, collagen fibrils are bundled together in a parallel formation to create fibers. These fibers then align together to form primary fiber bundles. As shown in figure 5 below, this hierarchical configuration continues to form a whole tendon.

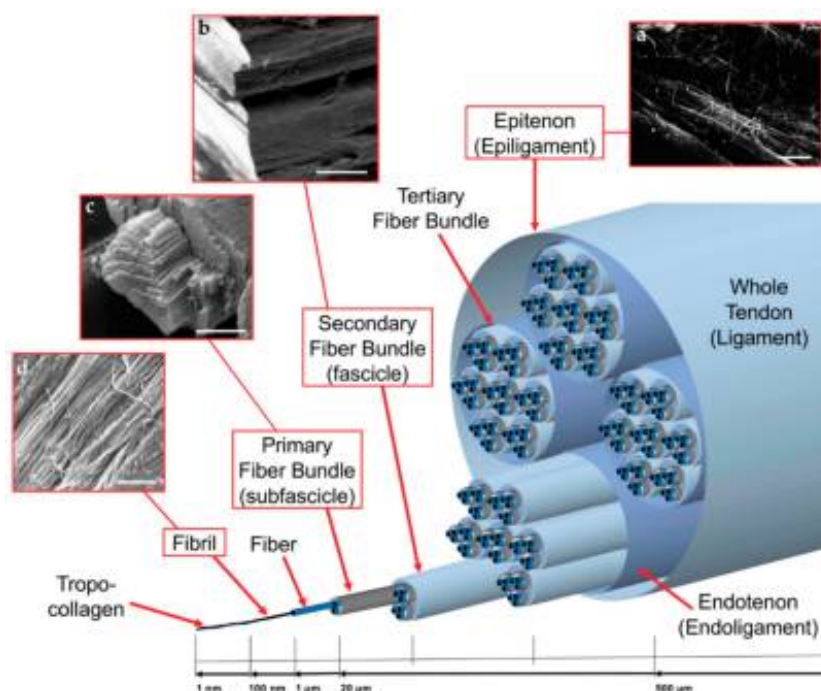


Figure 5: Structure of a Tendon (Sensini & Cristofolini, 2018)

In addition to the collagen, tendons are also made up of a large percentage of water and cells such as fibroblasts and tenocytes (Sensini & Cristofolini, 2018). Tendons are viscoelastic, meaning that they can exhibit both viscous and elastic mechanical behavior, which can be observed in their stress-strain curve. When the strain on a tendon is below 2%, the collagen fibers within the tendon are “crimped”, meaning that they are folded back and forth on themselves. In this stage, referred to as the “toe” region, the tendon fibers are less stiff and are able to absorb energy. When strain is above 2% and below 4%, the collagen fibers in the tendon have straightened out and the curve enters the “linear” region. In this region, the tendon is stiffer and experiences elastic deformation. Young’s Modulus of the tendon can be measured as the

slope of this linear region. Past 4% deformation, the tendon begins to experience some microscopic tears, which will increase as the strain increases until the tendon ruptures at around 8-10% deformation (Wang, et. al. 2012), (Sensini & Cristofolini, 2018). The ultimate tensile stress of a tendon can vary from about 24 to 112 MPa, as seen in figure 6 below of a generalized stress-strain curve of a tendon.

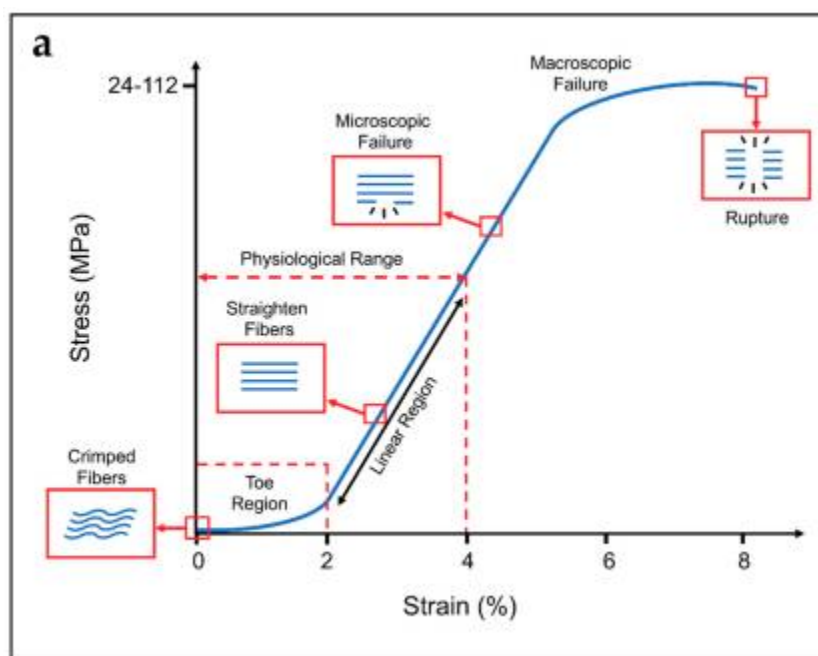


Figure 6: A typical stress-strain curve for tendons (Sensini & Cristofolini, 2018)

Tendon properties can vary greatly with a range of factors. Tendons can differ depending on the location, function, and age of the tendon (Wang, et. al. 2012). Even different regions of the same tendon can have varied mechanical properties. For instance, a study done by Matsushashi et. al. investigated the differences between the anterior and posterior subregions of the supraspinatus tendon. They found that, in addition to size differences, the anterior and posterior subregions of the tendon also had differing modulus of elasticity and ultimate stresses (2014). The properties of this tendon are displayed in table 1 below.

Table 1: Mechanical Properties of the Supraspinatus Tendon

Subregion of Tendon	Modulus of Elasticity (MPa) ± standard deviation	Ultimate Stress (MPa) ± standard deviation
Anterior	592.4 ± 237.4	22.1 ± 5.4
Posterior	217.7 ± 102.1	11.6 ± 5.3

Based on the results of this particular study, it is clear that the anterior region of the supraspinatus tendon has a much higher modulus and higher ultimate stress compared to the posterior region of the tendon. The researchers propose that this difference is likely due to the fact that the anterior region of the tendon takes on a much higher portion of the loading from the muscles, which requires it to be stronger. Another important factor to note is the relatively large standard deviations for each of these material properties. The researchers do not address the high variation in material properties of the tendons. It is possible that the variation is due to the fact that the study only tested seven supraspinatus tendons, which were retrieved from both male and female individuals from a wide range of ages (68.3 years +/- 15 years). According to Sensini & Cristofolini, 2018, “It is well established that the mechanical properties of tendons and ligaments decrease according to the age of the patients and tend to become stiffer” meaning that the large range in ages of the specimens may have contributed to the large range in material property data.

2.1.3 Ligaments

Ligaments are the soft tissues that connect bone-to-bone, allowing for stabilization within the joints. Although they are functionally different from tendons, ligaments have very similar mechanical structures and properties. Like tendons, the main structural component of ligaments is the collagen fibers, which are arranged in parallel bundles within a hierarchical structure (*see figure 5*). In addition to these fibers, there are also water and cells within the ligament. The similar structure and material composition results in ligaments having a stress-strain curve similar to those of tendons (*Sensini & Cristofolini, 2018*).

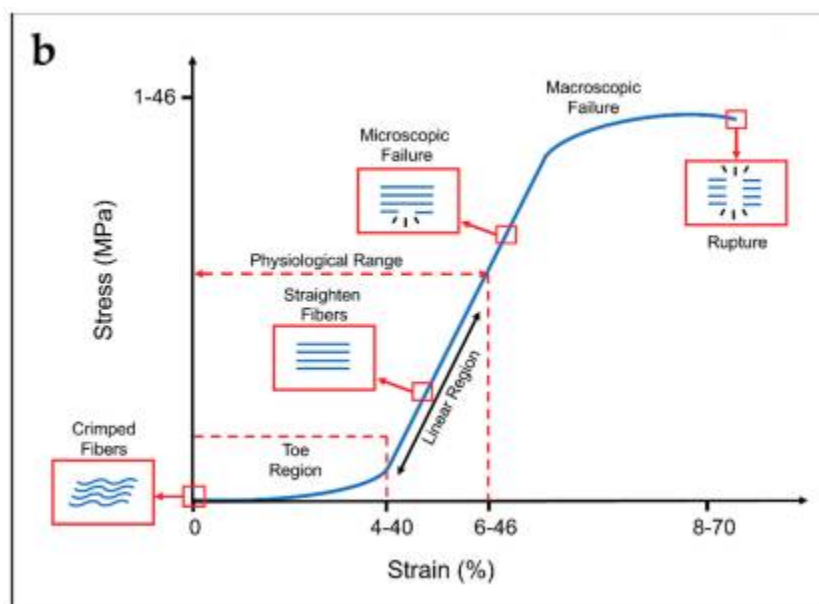


Figure 7: A typical stress-strain curve for ligaments (Sensini & Cristofolini, 2018)

While the shape of the stress-strain curve for ligaments (figure 7) is very similar to that of tendons (figure 6) there are a few key differences. For instance, the typical ultimate stress for ligaments can range from one to 46 MPa, while for tendons the ultimate stress can range from 24 to 112 MPa. Additionally, ligaments can have higher strains than tendons. From figure 7, the strain at failure for ligaments can be anywhere from 8% to 70%, while for tendons the strain at failure is typically 8% to 10%. Similarly to tendons, the mechanical properties of ligaments can vary greatly depending on the location and function of the ligament within the body (Sensini & Cristofolini, 2018).

Another important characteristic of ligaments is that their mechanical properties can vary under different loading conditions. Injuries to ligaments typically occur at high strain rates, so it is helpful to understand their mechanical behavior at high strain rates when considering shoulder injuries. The study tested the acromioclavicular ligament (AC), the coracoclavicular ligament (CC), and the sternoclavicular ligament (SC) under three different loading conditions (two high and one very low strain rate). The researchers found that with higher strain rates, Young's modulus and ultimate stress of the ligaments increased significantly when compared to the low strain rate (Koh, 2004). These differences can be seen in table 2 below which summarize the results of the study.

Table 2: “Summary of Mechanical and Structural Mean Values (+/- standard deviation) of 83 shoulder joints at three different strain rates and two high rates combined” (Koh, 2004)

	Strain rate	Deflection at failure (mm)	Load at failure (N)	Strain at failure (%)	Stress at ligament failure* (MPa)	Young's modulus (MPa)
AC (N=32)	High rate 1 (N = 13)	15 (+/- 4.0)	696 (+/- 218.3)	105 (+/- 20)	6.0 (+/- 1.0)	10.6 (+/- 1.7)
	High rate 2 (N = 10)	13 (+/- 7.1)	849 (+/-297.1)	81 (+/- 35)	7.8 (+/- 3.7)	9.6 (+/- 4.5)
	High rate 1 + High rate 2 (N=23)	14 (+/- 5.0)	761 (+/-274.0)	94 (+/- 27)	6.2 (+/- 1.8)	10.4 (+/- 2.8)
	Quasi static rate (N = 19)	11 (+/- 2.1)	464 (+/- 101.1)	80 (+/- 17)	3.4 (+/- 0.9)	6.3 (+/- 1.2)
CC (N=31)	High rate 1 (N = 12)	17 (+/- 7.6)	389 (+/- 194.1)	86 (+/- 34)	4.2 (+/- 1.6)	10.0 (+/- 3.8)
	High rate 2 (N = 10)	14 (+/- 4.3)	345 (+/- 132.1)	58 (+/- 18)	3.2 (+/- 0.9)	9.0 (+/- 3.8)
	High rate 1 + high rate 2 (N=22)	15 (+/- 6.4)	373 (+/-163.7)	72 (+/- 31)	3.9 (+/- 1.4)	9.6 (+/- 3.6)
	Quasi static rate (N = 9)	14 (+/- 4.0)	155 (+/- 80.2)	79 (+/- 39)	1.8 (+/- 1.0)	3.4 (+/- 1.8)
SC (N=20)	High rate 1 (N = 5)	12 (+/- 3.5)	670 (+/- 406.9)	62 (+/- 19)	n/a	10.2 (+/- 2.8)
	High rate 2 (N = 7)	13 (+/- 3.6)	604 (+/- 254.7)	50 (+/- 13)	n/a	12.7(+/- 2.3)
	High rate 1 + high rate 2 (N=12)	13 (+/- 3.4)	632 (+/-311.1)	55 (+/- 16)	n/a	11.7 (+/- 2.7)
	Quasi static rate (N = 8)	8 (+/- 2.4)	334 (+/- 143.7)	39 (+/- 10)	n/a	6.2 (+/- 0.6)

Foot notes:

AC: Acromioclavicular ligament CC: Coracoclavicular ligament SC: Sternoclavicular ligament

*Stress at ligament failure includes only those samples that failed at the ligament

n/a: Sternoclavicular joint did not have ligament failure

2.1.4 Muscles

Muscles are soft tissues that convert chemical energy into mechanical energy to help the body perform essential functions (Frontera, 2014). Some of these functions include movement, breathing, digestion, moving blood throughout the body, etc. Skeletal muscles are voluntary muscles, meaning their function can be controlled, and they work with tendons and ligaments to actuate movement. Muscles are composed of many small fibers, called myofibrils when bundled together. A bundle of myofibrils creates a muscle fiber, and a bundle of muscle fibers creates a

muscle. Muscles are connected to bone on either end by tendons (Frontera, 2014). Figure 8 below shows the structure of muscles.

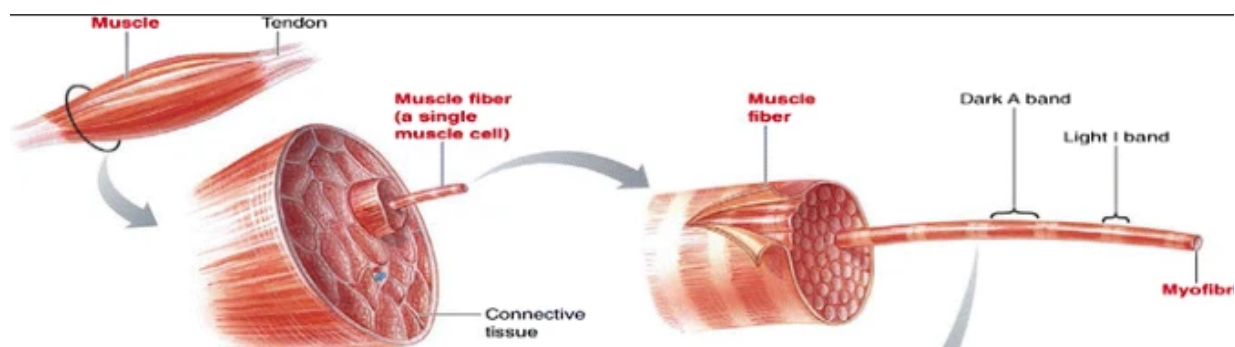


Figure 8: Structure of a muscle (Frontera, 2014)

The mechanical properties of muscles can vary in the body, and the properties of the same muscles can change as a response to movement. The previous MQP team's iteration consisted of five muscles, the supraspinatus, upper trapezius, lower trapezius, serratus anterior, and deltoid. A variety of research studies of these muscles are discussed below.

A study using Ultrasound Shear Wave Elastography evaluated how the elastic modulus of shoulder muscles changes in response to the baseball pitch motion. The elastic modulus of the supraspinatus, infraspinatus, middle trapezius, lower trapezius, rhomboids, and serratus anterior muscles were evaluated before, immediately after, and 24 hours after the participants completed a baseball pitch (see table 3 for results). Before throwing, the elastic moduli range from $19.2 \text{ kPa} \pm 6.4 \text{ kPa}$ in the serratus anterior to $45.1 \text{ kPa} \pm 27.2 \text{ kPa}$ in the middle trapezius. Immediately after throwing, the elastic moduli of the muscles increases, and then lowers 24 hours after throwing, but does not quite return to the original resting elastic modulus (Yamaura, 2021). This study provided useful information about the properties of the supraspinatus, lower trapezius, and serratus anterior (highlighted in the table below) to aid in the material selection for muscles.

Table 3: Elastic modulus (in kPa) of shoulder muscles before pitching, immediately after, and twenty-four hours after (Yamaura, 2021).

Muscle	Elastic Modulus before throwing	Elastic Modulus immediately after throwing	Elastic Modulus 24 hours after throwing
Supraspinatus	32.9 ± 15.7	53.4 ± 20.9	43.8 ± 22.2
Infraspinatus	22.7 ± 10.3	44.8 ± 26.8	43.7 ± 25.9
Middle Trapezius	45.1 ± 27.2	70.3 ± 26.8	59.9 ± 25.5
Lower Trapezius	32.8 ± 13.3	45.5 ± 15.6	46.5 ± 23.9
Rhomboideus	29.1 ± 19.6	47.5 ± 24.6	38.8 ± 16.6
Serratus Anterior	19.2 ± 6.4	36.9 ± 9.9	26.5 ± 10.2

In another research study, the effects of abduction on the elastic modulus of the upper trapezius was investigated. It was found that the upper trapezius has an elastic modulus of 17.11 ± 5.82 kPa while at rest and 26.56 ± 12.32 at 30 degrees of abduction (Leong, 2013). The full results of this study are shown in table 4 below. These elastic moduli are comparable to the elastic moduli of the muscles evaluated in Yamaura's study shown above, with the elastic modulus of the upper trapezius showing similarity to the elastic modulus of the serratus anterior.

Table 4: Elastic modulus of the upper trapezius both at rest and at 30° of abduction (Leong, 2013).

	Shear Elastic Modulus Mean ± SD (kPa)
Arm at Rest	17.11±5.82
Arm at 30° abduction	26.56±12.32

Another study investigated the effects of elongation on the elastic modulus of different segments of the deltoid muscle, which are shown in figure 9 below. It was found that the middle deltoid has a modulus of 63.0 ± 13.1 kPa at an elongation of 0 mm (Hatta, 2016). The full results of this study are shown in table 5 below.

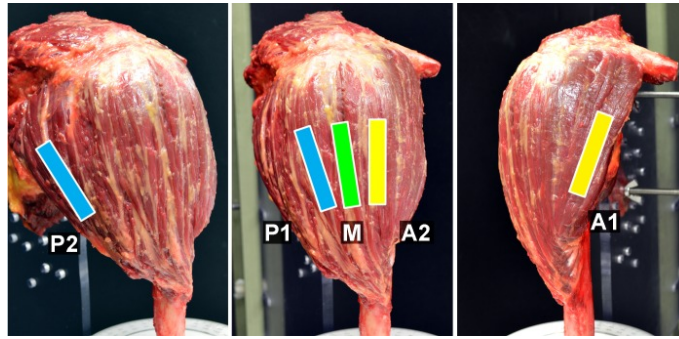


Figure 9: Regions of deltoid muscle referenced (Hatta, 2016).

Table 5: Elastic modulus (in kPa) of five regions of the deltoid muscle (A1, A2, M, P1, P2) at elongation lengths of 0 mm, 5 mm, 10 mm, 15 mm (Hatta, 2016).

	0 mm	+5 mm	+10 mm	+15 mm
A1	55.9±8.9	60.3±11.1	71.2±10.8	76.2±11.6
A2	72.4±9.1	77.6±9.8	109.9±20.0	129.3±34.9
M	63.0±13.1	69.7±15.7	97.4±12.1	123.5±33.9
P1	50.2±9.9	57.2±17.5	71.4±14.9	89.0±27.1
P2	39.1±11.9	42.8±13.3	52.2±15.4	61.3±14.4

The elastic modulus of the five muscles in the prior MQP team's iteration (the serratus anterior, upper trapezius, lower trapezius, middle deltoid, and supraspinatus) are represented in these studies and summarized in table 6 below. While there is variation in the elastic modulus between muscles, and even within the same muscle, the values are all in the same order of magnitude. This means it may be possible to represent all of the muscles in the model with a material that has an elastic modulus in that same order of magnitude.

Table 6: Summary table of the elastic modulus of the five muscles represented in the current model (Yamaura, 2021; Leong, 2013; Hatta, 2016).

Muscle	Elastic Modulus (kPa)
Serratus anterior	19.2±6.4
Upper trapezius	17.11±5.82
Lower trapezius	32.8±13.3
Middle deltoid	63.0±13.1
Supraspinatus	32.9±15.7

2.1.5 Tendon Attachment to Bone

The enthesis, also referred to as insertion sites, is the area where tendons and ligaments attach to the bone. The main function of the enthesis is to transmit forces from the skeletal muscle to the bone, creating mobility of the musculoskeletal system. Mechanical stress is concentrated at these sites and transferred between the soft and hard tissues. (Aghaei, 2020). These soft and hard tissues can be classified into two categories, fibrous or fibrocartilaginous, depending on the tissues present (Benjamin, 2006). The fibrous enthesis is where the tendons and ligaments attach to the shaft of long bones, which are bones with two ends that are longer than wide. In the shoulder, this would include the humerus (Aghaei et al., 2021). The fibrocartilaginous enthesis is more commonly present at bony attachments, such as the rotator cuff. Fibrocartilaginous enthesis has four regions (or hierarchical levels): the tendon region, non-mineralized fibrocartilage region, mineralized fibrocartilage, and bone. Throughout these four regions, different types of collagen fibers are present, affecting the mechanical properties. These regions are shown in figure 10.

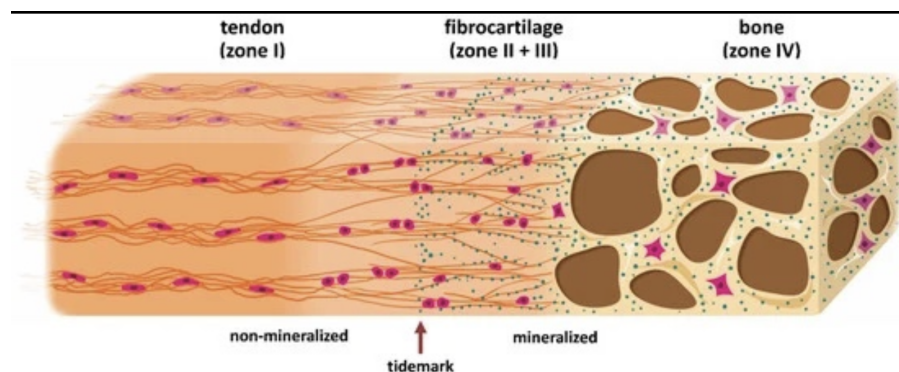


Figure 10: Layers of the enthesis

In addition to these four regions, the entheses have gradients at the interface regions, shown microscopically in figure 11 below. The gradients smooth stress distribution, eliminate singularities in stress, reduce stress concentration, improve bonding strength, and decrease the risk of fractures (Benjamin, 2006).

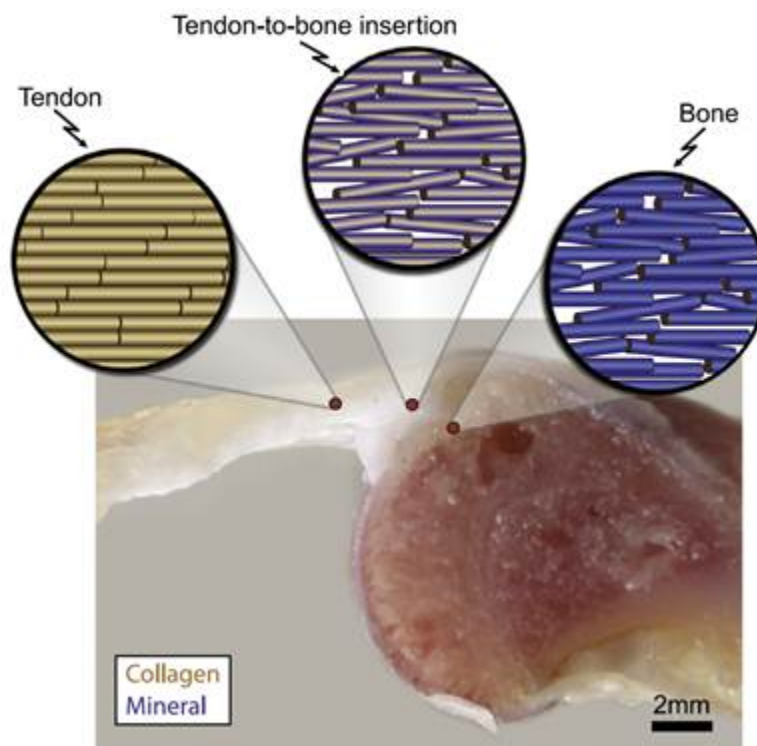


Figure 11: Gradients of the entheses regions (Schwartz, 2013)

The mechanical environment of the enthesis is complex and heterogeneous since the enthesis is subjected to tensile, compressive, and shear forces. Force transmission across

entheses are also very high, since muscles attach to the bones close to the axis of motion, resulting in small lever arms and higher forces needed to produce the required torque. An example of this is the biceps which has a lever arm 1/10th of the center of mass of the forearm, meaning the muscle needs to generate over ten times the weight of the forearm for elbow flexion (Avin et al., 2015). There are several characteristics of the entheses that allow them to withstand these large and complex forces. For instance, as tendons approach the insertion sites, the mechanical properties change (Porczink, 2003). The enthesis also has a shallow attachment angle and optimized shape to improve resistance to mechanical loads. Additionally, tendons and ligaments flare out at attachment sites which allow them to have a secure attachment to the skeleton and resist the effects of angle change (Avin et al., 2015). The security of these attachment points is critical due to the forces they must withstand.

2.1.6 Recent Developments in Soft Tissue Replication

Even though the entheses are very important for force transmission from tendons and ligaments onto the skeleton, they are not commonly studied, and therefore there is a lack of understanding of healthy attachments. Tendon ruptures that require surgical reattachment have a high failure rate because the structural integrity of the enthesis is rarely regained. The enthesis rarely regenerates by itself or from using current rehabilitation methods and thus does not recover its mechanical properties (Aghaei et. al., 2021). To counter this, many studies have focused on rehabilitation methods that can be implemented after a tendon operation. These methods target compositional and structural features at lower length scales (e.g. different collagen types) which would include collagen types. There have been attempts to measure the mechanical properties of the tendon-bone insertion, but it has proven to be difficult because of the heterogeneity and small dimensions of the enthesis.

Recent studies have attempted to improve tendons and repair them using biomaterials. John A. Paulson, Elkhart Weber, and Daniel Kauffman created the Janis Tough Adhesives (JTAs) which is a biomaterial-based tendon therapy (Irving, 2022). The JTA is a two sided biomaterial where one side adheres firmly to the tendon while the other side is smooth and allows for other soft tissues to glide around it. It is mechanically tough and elastic, allowing for it to follow the movement of the tendon without deforming or breaking. This adhesive helps with tissue

regeneration and facilitates healing as it reduces the mechanical load on a tendon and is able to release a drug that reduces inflammation. The JTA can be seen on a model tendon within a model joint, below, in figure 12. Similar tissue adhesives include TISSEEL, Dermabond, and SurgiCel (Irving, 2022).



Figure 12: Janis Tough Adhesive (blue) on a tendon model within a joint (Irving 2022)

Similarly, UCLA material scientists developed durable artificial tendons which were made to mimic the internal structure, stretchiness, strength, and durability of biological tendons. The UCLA scientists used hydrogels since they were on par with or stronger than natural biological materials (Newsroom 2021). The tendons are made of a hydrogel, which has the potential to be 3D printed and transformed into other shapes. It also has multiple structures similar to the biological tendons, making it stronger and more stretchable. The comparison between the layers of tendon material and the hydrogel can be seen in figure 13 below. All of these materials are relatively new and difficult to obtain, thus they were not selected for use in our project. However, researching these innovations has given important insights about the mechanics of tendon attachments which was used to inform the creation of our model.

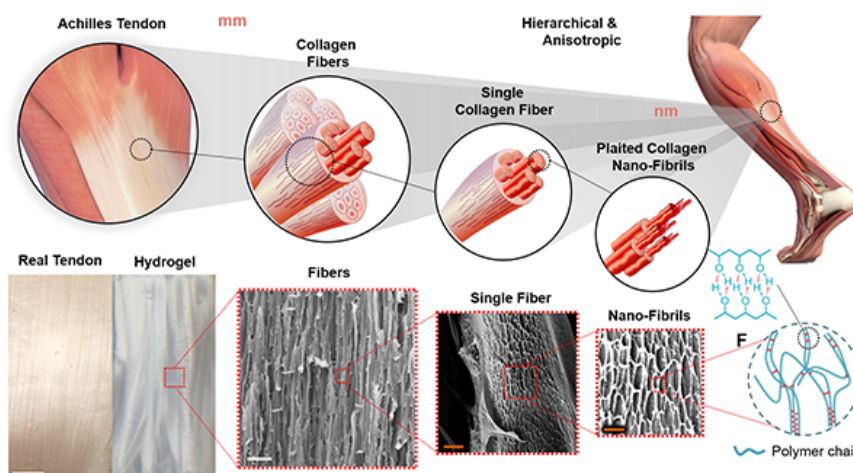


Figure 13: Hydrogel tendon material layer compared to real tendon attachment (Newsroom 2021).

2.1.7 Abduction

General Movement

Shoulder abduction is the movement of the arm away from the midline of the body in the sagittal plane (plane of the torso). The motion begins with the arm parallel to the torso and the hand in an inferior (downward) position. In the middle of the movement, the arm is perpendicular to the torso. Abduction ends with the humerus raised above the shoulder joint, pointing straight upward. The abduction angle is measured by the angle between the humerus and the midline of the body. This motion can be seen in figure 14 below.

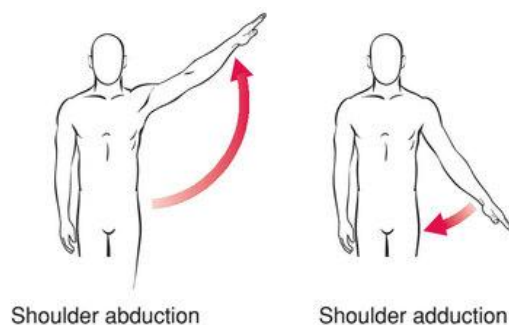


Figure 14: Shoulder abduction motion (Anatomy Language: Part II, 2014)

Main Acting Muscles and Force Vectors

There are four main muscles that contribute to shoulder abduction: the supraspinatus, deltoid, trapezius, and serratus anterior (Lam J.H. et al. 2021). The force vectors of these muscles

have both rotary and translatory components, which act together to rotate the shoulder and stabilize the joint (Schenkman & Cartaya 1987).

For the first 15 degrees of abduction, the supraspinatus is the primary muscle force in abduction. Past this first 15 degrees, the supraspinatus continues to contribute to shoulder abduction by providing stability in shoulder movement and resisting gravitational forces on the joint to keep the humerus in the glenoid fossa (Lam J.H. et al. 2021). The supraspinatus is part of a group of muscles called the rotator cuff muscles, which also include the subscapularis, infraspinatus, and teres minor (*Shoulder Anatomy*, n.d.). The rotary force of the rotator cuff muscles together rotates the humerus medially (towards the centerline of the body). The translatory force of the rotator cuff muscles pulls the humerus downward (Schenkman & Cartaya 1987).

Between 15 and 90 degrees of abduction, the deltoid is considered the primary moving force in abduction (Lam J.H. et al. 2021). The rotary component of the deltoid rotates the humerus outward while the translatory component pulls the humerus upward, towards the acromion. Since the deltoid pulls the humerus upward while the rotator cuff pulls down, the resulting force stabilizes the humeral head in the glenoid fossa. Meanwhile, the rotary components of the deltoid and rotator cuff form a force couple, as seen in figure 16 (Schenkman & Cartaya 1987).

Beyond 90 degrees, the trapezius and serratus anterior work together to move the scapula and facilitate shoulder abduction. Specifically, the trapezius is responsible for the upward rotation, elevation, and external rotation of the scapula, while the serratus anterior contributes to the upward rotation and internal rotation of the scapula. (Lam J. H. et al., 2021). These movements are illustrated in figure 15 below. In terms of force vectors, the upper trapezius and upper portion of the serratus anterior form one force couple while the lower trapezius and lower portion of the serratus anterior form another force couple. These force couples cause the scapula to first rotate around the axis of the scapular spine until the humerus reaches 90 degrees. Once the scapula has reached 30 degrees of upward rotation, the axis shifts to the point on the spine near the acromioclavicular joint. After this shift, the lower trapezius becomes the main rotary force (Schenkman & Cartaya 1987).

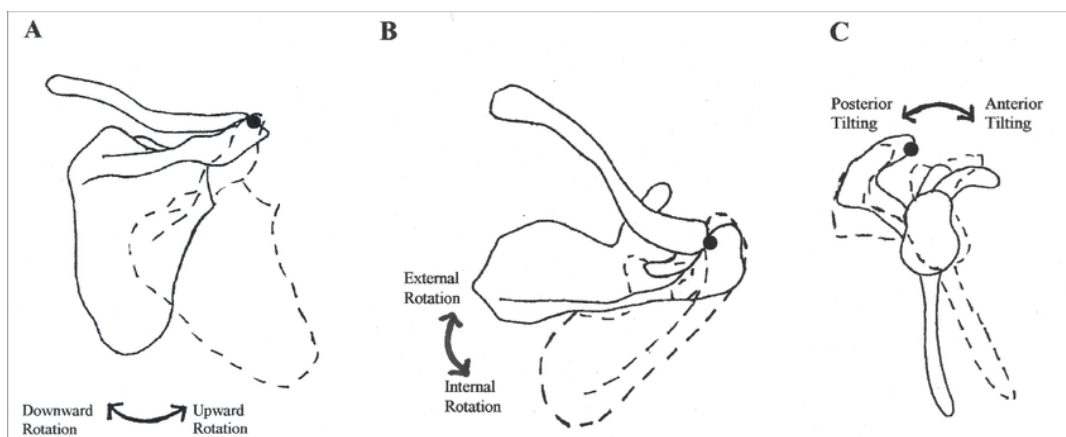


Figure 15: Rotation of scapula (Lee et. al, 2020)

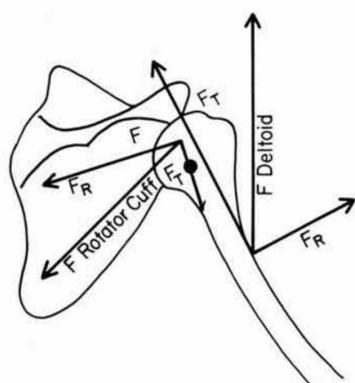


Fig. 3. Force couple of deltoid and rotator cuff muscles. The rotatory forces, acting on opposite sides of the axis of motion, combine to produce upward rotation. The translatory forces cancel each other out. F_R , rotatory force; F_T , translatory force.

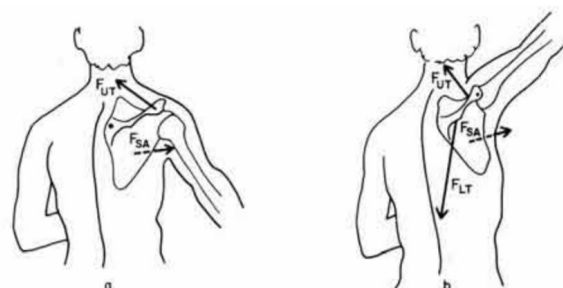


Fig. 4. Force couple of muscles acting at the scapula. F_{UT} , force of upper trapezius; F_{LT} , force of lower trapezius; F_{SA} , force of serratus anterior. a, Axis of scapular rotation from 0–30°; b, axis of scapular rotation from 30–60°.

Figure 16: Forces acting on the shoulder during elevation (Schenkman, M., & Rugo de Cartaya, V., 1987)

Scapulohumeral Rhythm

During abduction, the scapula and humerus bones move in what is known as the scapulohumeral or glenohumeral rhythm. The scapulohumeral rhythm describes the relative movement of the glenohumeral and scapulothoracic joints during elevation. This motion is pictured in figure 17 below. This rhythm is critical to the optimal function of the shoulder because it preserves the length-tension relationship of the glenohumeral ligaments. The rhythm also allows the muscles to sustain their force production since they do not need to shorten as much as they would if the scapula did not rotate. Lastly, the movement prevents the humerus and

acromion from impinging on each other since they move simultaneously in the same direction (Scapulohumeral Rhythm, *n.d.*).

The scapulohumeral rhythm is known to move the scapula and humerus together in a specific ratio. For the first 30 degrees of glenohumeral abduction, the scapula remains at rest. After this first 30 degrees, the glenohumeral and scapulothoracic joints move simultaneously in a 2:1 ratio. This means that after 90 degrees of glenohumeral abduction, there will be 30 degrees of scapulothoracic rotation (Scapulohumeral Rhythm, *n.d.*).

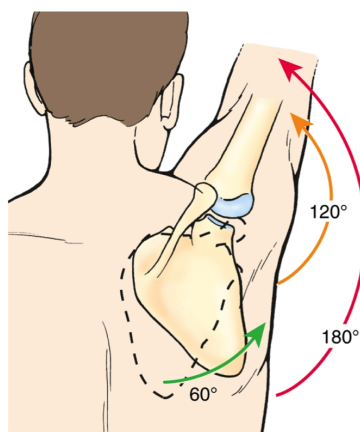


Figure 17: Scapulohumeral Rotation (Scapulohumeral Rhythm, n.d).

In addition to the upward rotation of the scapula, which is shown in the illustration above, the scapula also experiences posterior tilt and external rotation during shoulder abduction. All three directions of scapular rotation are shown in figure 15 above. The degrees at which the scapula rotations in these three directions can be related to the abduction angle of the humerus. A study by Lee et. al. took measurements of the scapula position from ten healthy participants as they abducted their shoulders (2020). The results of this study for active abduction between zero and 90 degrees is shown in the table 7 below:

Table 7: Scapula rotation based on humeral abduction angle (Lee et. al. 2020)

Abduction Angle (degrees)	Upward Rotation of Scapula (degrees)	Posterior Tilt of Scapula (degrees)	External Rotation of Scapula (degrees)
Start	8.2 ± 4.5	0	0
30	10.9 ± 4.6	1.7 ± 0.9	1.2 ± 1.6
45	17.3 ± 7.0	3.2 ± 1.6	2.1 ± 2.5
60	22.6 ± 8.7	4.6 ± 2.3	2.5 ± 2.7
75	26.4 ± 8.8	5.9 ± 2.3	2.8 ± 2.6
90	29.2 ± 7.8	7.5 ± 1.6	3.3 ± 2.9

We can see from this study that experimental data of scapula rotation holds somewhat accurate to the 2:1 ratio that was described earlier. In table 7 above, the column for “upward rotation of the scapula” matches well with the 2:1 ratio of the humerus and scapula for the range of 30 to 45 degrees. However, the experimental data does not match the 2:1 ratio exactly for all degrees of abduction. This is because the 2:1 ratio is a simplification of the average scapulohumeral rhythm and is not perfectly accurate, especially considering the variability of shoulder movement between individuals. Despite the fact that this 2:1 ratio is a simplification, we still chose to use this as the ideal rhythm for our model.

This study also gives insight into the posterior tilt and external rotation of the scapula during abduction. At 90 degrees of glenohumeral abduction, the scapula has a posterior tilt of 7.5 ± 1.6 degrees and an external rotation of 3.3 ± 2.9 degrees. This information was helpful for evaluating the movement of our model, since we were able to see how our scapula moved compared to the experimental data.

2.2. Prior Team’s Model

2.2.1 Motor Placement

Previously, the motors actuating the deltoid and supraspinatus muscles were attached to the humerus (see figure 18).



Figure 18: Previous model's motor placement

The previous group used the free body diagram shown in figure 19 below to calculate the force that the deltoid muscle would need to lift, given this motor placement. A description of the variables used are shown in table 8. Each of these motors weighed about 0.88 lb, while the weight of the 3D-printed humerus was only 0.547 lb. Thus the additional weight of the motors more than quadrupled the total weight of the humerus. This excessive weight on the humerus resulted in excessive force required from the supraspinatus and deltoid muscles, which both work to rotate the humerus about the humeral head. This high force in the muscles likely contributed to the plastic deformation in the muscle material.

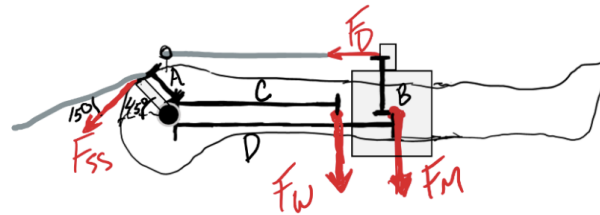


Figure 19: Free body diagram of forces on the humerus with current model placement.

Table 8: Variable descriptions for free body diagrams (Deane et al, 2022).

Variable	Description
A	Distance from supraspinatus insertion point to center of rotation of the humeral head
B	Distance from the central axis of the humerus to the axis to the line of action of the deltoid
C	Distance from the center of rotation of the humeral head to the center of mass of the humerus
D	Distance from the center of rotation of the humeral head to the location of the motors (previous model) or attachment point of the deltoid muscle (new motor placement)
Fw	The weight of the 3D printed humerus
Fss	Force of the supraspinatus
Fm	Weight of two Nema 17 motors (previous model only)
Fd	Force of the deltoid

2.2.2 Soft Tissues Materials and Placement

The previous team chose to focus on the soft tissues most needed for the abduction movement, and they simplified them as linear attachments. The simplified attachment points are anatomically accurate; however, they had chosen to forego material properties in the interest of time constraints.

The previous iteration of the model included the five muscles primarily used in abduction: serratus anterior, trapezius (upper and lower are included), middle deltoid, and supraspinatus. For simplicity, adduction was modeled as abduction in reverse. In reality, adduction is completed with a different set of muscles (pectoralis major, latissimus dorsi, teres major, triceps, coracobrachialis). Because the model's main focus is abduction, mechanical accuracy in adduction was sacrificed for the time being. These muscles were replicated with fishing lines and actuated with motors. The fishing line was chosen because it was flexible enough to wrap around the spool of a motor and had a low coefficient of friction, which allowed it to easily slide over PLA bones and through silicon tubes without damaging them. However, the

fishing line plastically deformed easily, which led to inaccuracies in forces and scapulohumeral rhythm over time. Reducing the ductility of muscles and attachments is a priority for this project. Another factor contributing to inaccuracies in the scapulohumeral rhythm was the lack of stabilizing muscles. Many of the muscles used in adduction, which were left out of the model, also play a stabilizing role during abduction.

The glenohumeral joint capsule ligaments and acromioclavicular (AC) ligaments were included in the previous team's model and were replicated with bungee cords and KT tape/fishing line respectively. In the glenohumeral joint capsule, the superior, middle, inferior, and spiral glenohumeral ligaments were included, as well as the coracoclavicular and coracohumeral ligaments (simplified as one linear attachment) and the coracoacromial ligament. The attachment points of the bungee cords were not anatomically accurate due to material limitations; however, the directions of the stabilizing forces replicated with the bungee cords were accurate. The KT tape used for the acromioclavicular ligament capsule allowed for flexibility and had good adherence to the PLA used for bones. A braided fishing line was also used as a cushion, spacer, and lubricant. We chose to focus on improving the glenohumeral ligaments for this project because the KT tape and fishing line combination worked well for the AC.

2.2.3 Attachment Methods

There are a few different types of attachments needed in the model: tendons to bones and ligaments to bones. The prior MQP replicated the attachments of tendons to bones in a few different ways. One method they used for attachment points located at the edges of bone involved drilling holes through the bone at the attachment point. The fishing line was strung through the hole and tied (see figure 20). Eye hooks were also used to adjust the direction of the fishing line to replicate the line of action of the muscle force (see figure 21). Motors were used to actuate the muscles. To attach the fishing line to the motors, it was tied and wound around the spool.

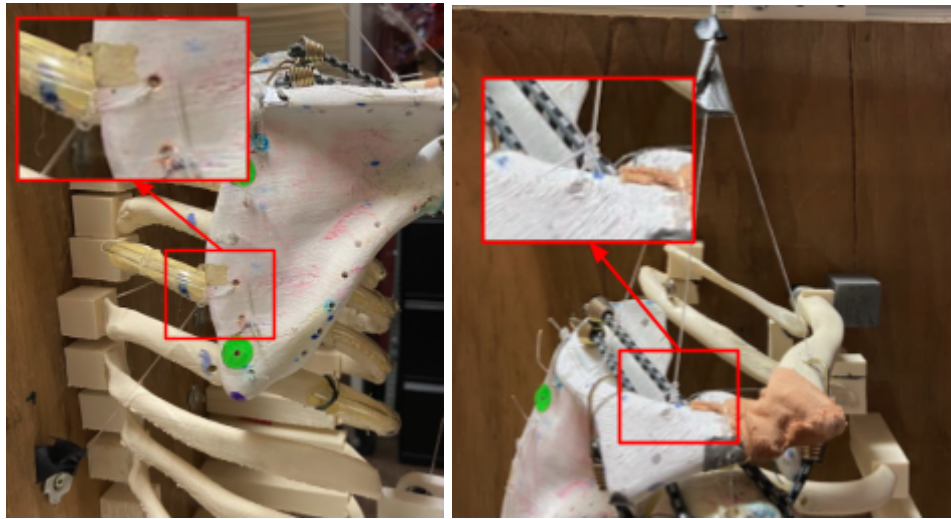


Figure 20: The drilling method used for muscle attachment points. The attachment points of the lower trapezius (left) and upper trapezius (right) are shown to illustrate this method.

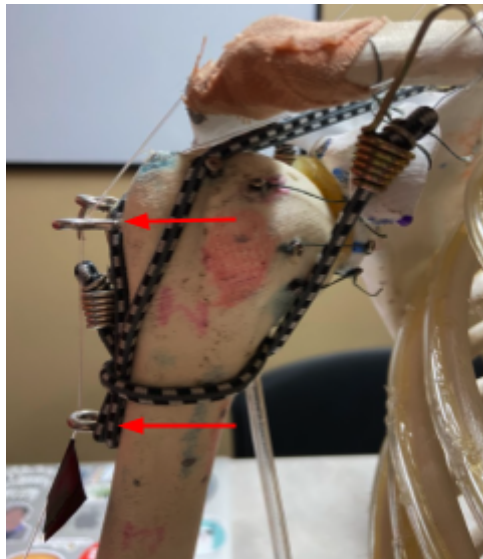


Figure 21: Eye hooks were used to achieve the proper line of action of the deltoid muscle.

The prior MQP also needed to replicate ligament attachment points. For the attachment points of the acromioclavicular ligament capsule, KT tape was used. The adhesive of the KT tape adhered well to the PLA of bone (see figure 22). The bungee cords used to replicate the glenohumeral joint capsule ligaments were attached by drilling holes in the PLA bones and inserting the hooks of the bungee cords into them, as well as by inserting eye hooks into the bone and attaching the bungee cords to those (see figure 23).



Figure 22: KT Tape used to replicate the acromioclavicular ligament capsule.

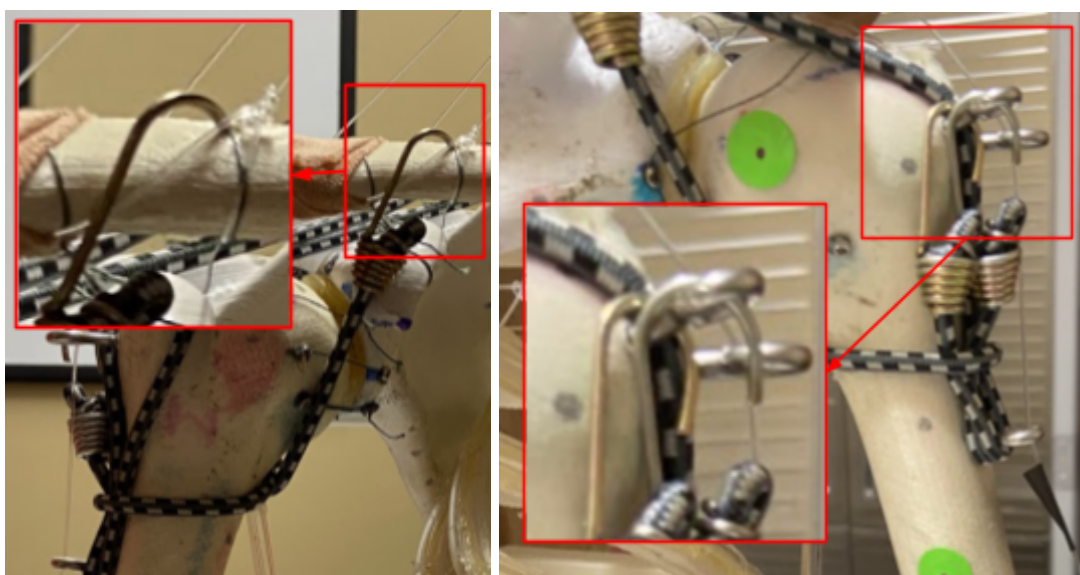


Figure 23: Attachment points of bungee cords.

3. Methodology

3.1 Building Methods

3.1.1 Build goals

Building off of the existing model from the previous MQP team, our project had three main goals: adjust motor locations and muscle vectors, select more biologically accurate materials to replicate soft tissues, and improve attachment methods.

Motor Location and Function

1. Relocate the deltoid and supraspinatus motors so that they do not put excess weight on the arm of the model.
2. Create biologically accurate force vectors based on the force vectors of real muscles
3. Measure the change in length of all muscles throughout the abduction movement and utilize this information in coding of motors

Material selection for tendons, muscles, and ligaments

1. Select materials that mimic biological tissues with comparable material properties such as elastic moduli and viscoelasticity.
 - a. Select muscle materials that have an elastic modulus in the range of 0.017 to 0.063 MPa, tendon materials that have an elastic modulus in the range of 217.7 to 592.4 MPa, and ligament materials that have an elastic modulus in the range of 3.4 to 6.3 MPa.
 - b. Select materials with stress-strain curves that match the shape of the stress-strain curves for natural tendons and ligaments with a toe region before the linear region.
2. Select materials that can be incorporated into the physical model.
 - a. Select materials that will ensure longevity and functionality of the model by having yield strength higher than the anticipated stresses.

- b. Select materials with low friction and sufficient pliability so that they do not hinder the movement of the model (e.g. the muscles need to be able to slide easily on the bones and form to the bones where necessary).

Improve attachment methods

1. Manufacture attachments that transmit forces between bone, tendons, and muscles while avoiding stress concentrations at attachment sites.
2. Create tendons that flare out at attachment sites to better mimic the enthesis region and allow for secure attachments.
3. Place tendon to bone attachment sites closer to the bone to eliminate the gap between the tendon and bone present in the previous model and to allow for more accurate directions of muscle forces.

3.1.2 Material Selection for Soft Tissues

Evaluation Criteria

When beginning our material selection process, we considered several criteria which were important to our project. Our top two criteria for material selection were biological accuracy and resistance to plastic deformation which aligned with our overall project goals. Cost, manufacturability, and time were the next most important qualities that we considered since they contributed to the feasibility of building our final model. Due to budget and time limitations, it was crucial that the chosen materials were cost effective, time efficient, and easily manufactured. With these factors in mind, we considered several materials, including PLA, Nylon, TPU, Objet Tango Black, Formlabs Flexible, Formlabs Elastic, Moldstar 30 Silicone Rubber, and rubber exercise bands. All of these materials were able to be 3D printed on WPI's campus with the exception of the Moldstar 30 Silicone Rubber and rubber exercise bands, which would need to be purchased from outside suppliers. These materials were selected based on the criteria from our own background research (see sections 2.1.2, 2.1.3, and 2.1.4) as well as suggestions from the previous team.

Each material considered was evaluated by our five criteria, allowing us to arrive at our top three options: thermoplastic polyurethane (TPU), Formlabs Elastic, and Formlabs Flexible.

The Formlabs Elastic and Flexible materials are both soft elastomeric resins. The exact composition for Formlabs Elastic and Formlabs Flexible material is not known as it is proprietary information kept by Formlabs. These materials were chosen because they were able to be 3D printed on campus, meaning they were quick and easy to manufacture. They were also all relatively low cost, with the TPU costing about \$0.10 per gram and the Formlabs materials both costing about \$20-30 per cubic inch. We also found that these materials would be resistant to plastic deformation under the loads applied in the model. However, further material testing was required to show if these materials properly mimicked biological soft tissues. For our preliminary material evaluation process and the other materials we considered, see appendix 9.4.

Tensile Testing

Tensile testing of our top three materials (TPU, Formlabs Flexible, and Formlabs Elastic) was performed to ensure that each material could withstand the forces in the model. We also compared their stress vs strain curves to those of the natural soft tissues to evaluate if they would mimic the natural soft tissues' properties well.

The tensile testing machine used to complete these tests was the Mecmesin MultiTest 2.5-dv(U). Figure 24 shows the tensile testing set-up. We used ASTM D638, the Standard Test Method for Tensile Properties of Plastics, to guide our testing procedure (ASTM Standard D638, 2022). See appendix 9.8 for the exact testing procedure. Our first step when following the ASTM testing procedure was to determine which type of test specimen would best fit the types of materials we were testing. We were testing a non-rigid plastic with a thickness of 4 mm or less, so we chose the Type IV specimen (see figure 25 and table 9).

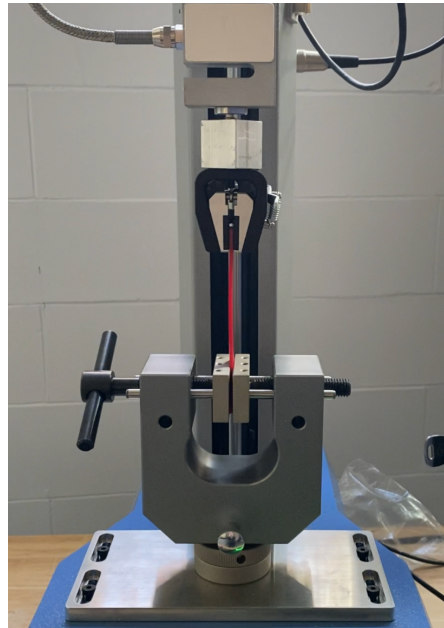


Figure 24: Tensile testing set-up.

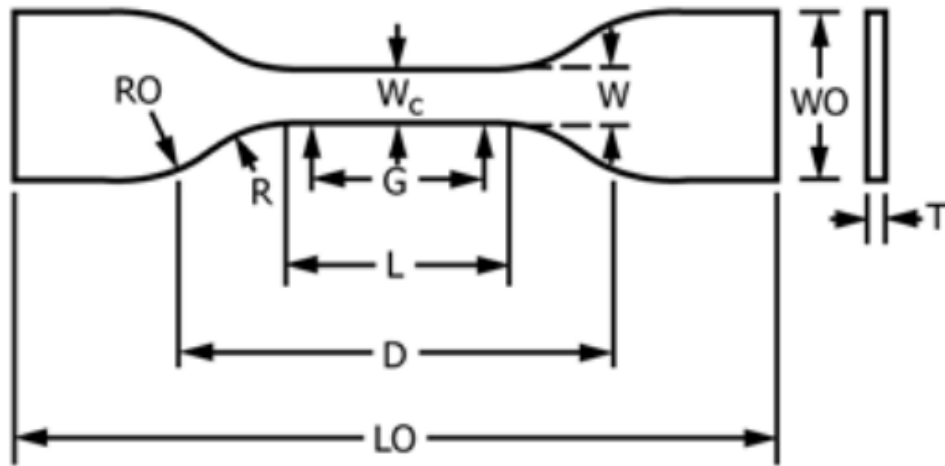


Figure 25: Tensile testing specimen with 2mm thickness

Table 9: Tensile testing specimen dimensions.

Variable	LO	D	L	RO	R	W	WO	T
Dimension (mm)	115	65	33	25	14	6	19	2

We 3D printed two samples of each material so that we could test until failure and obtain full stress-strain curves for each material. We performed one test on each material. Each test was performed at a strain rate of 50 mm per minute which complied with the ASTM standard.

Testing until failure gave us insights into how these materials behave. TPU was able to withstand the maximum force of the testing apparatus (almost 300 N, for a resulting stress of almost 25 MPa), reached a maximum strain of 570%, and had an elastic modulus of 437 MPa. The TPU specimen did plastically deform; however, the plastic deformation only began after 5 MPa (see figure 26). Formlabs Elastic was able to withstand about 70 N of force before failure, it had an elongation at failure of 170%, and it had an elastic modulus of 8 MPa (see figure 27). Formlabs Flexible was able to withstand about 35 N of force before failure, it had an elongation at failure of 205%, and it had an elastic modulus of 2 MPa (see figure 28). The Formlabs Elastic and Flexible materials did not experience any plastic deformation, they only elastically deformed until failure. See figure 29 for comparisons of the three samples.

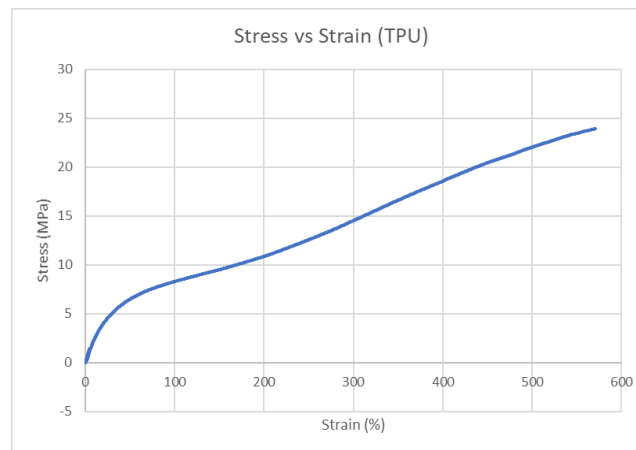


Figure 26: Stress vs strain curve generated by tensile testing TPU at a speed of 50 mm/min until failure.

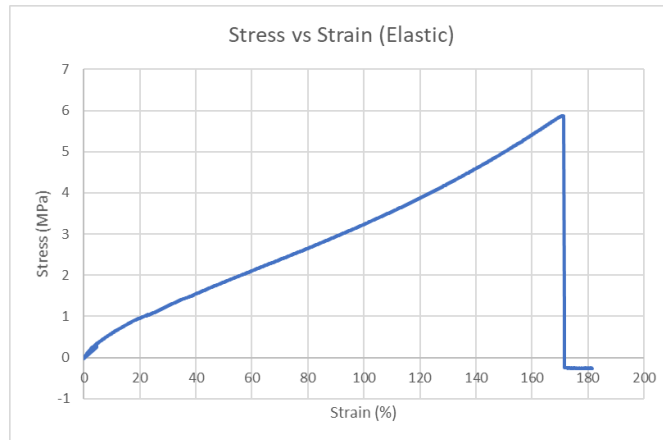


Figure 27: Stress vs strain curve generated by tensile testing Elastic at a speed of 50 mm/min until failure.

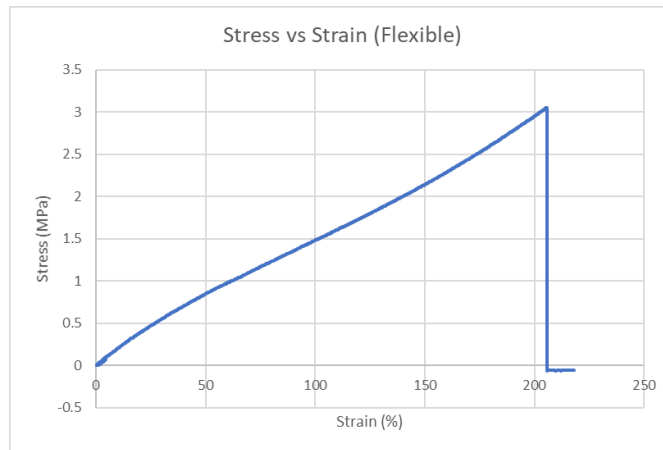


Figure 28: Stress vs strain curve generated by tensile testing Flexible at a speed of 50 mm/min until failure.



Figure 29: Comparisons of the TPU, flexible, and elastic materials. TPU1, F1, and E1 were subjected to tensile testing, while TPU2, F2, and E2 were not.

Having tested the samples until failure, we then calculated the ductility of each material by finding the change in length after testing and dividing that by the original length. The original gauge length of all specimens was 65 mm, based on the ASTM standards that we followed. TPU did not achieve failure with the tensile testing machine available to us. However, after tensile testing we measured the gauge length of the TPU to be 80 mm, giving it >23.08% ductility. As stated before, Formlabs Flexible and Elastic experienced almost no plastic deformation during tensile testing. Each of the Formlabs materials were measured to have a gauge length of about 65 mm after tensile testing, giving them 0% ductility. TPU had a much higher fracture strength than the other two materials, since the TPU was not able to be fractured by the maximum force of the tensile testing machine.

Tendons

We chose TPU to represent tendons in our model because it possessed a similar elastic modulus to biological tendons. In the literature, we found that the elastic modulus of tendons in the shoulder can range from approximately 115 to 830 MPa (see table 1). In our tensile testing of

the TPU we found an elastic modulus of approximately 437 MPa (see figure 26), which is well within this range. Additionally, from our tensile testing, we observed that TPU did not begin to plastically deform until approximately 5 MPa of stress had been applied, which is well above the stresses that would be present in the model. We also know that the ultimate stress of TPU would be more than sufficient, since the ultimate stress of TPU in our experiment was found to be >25MPa, while the ultimate stress of biological shoulder tendons is 11-22 MPa. Since TPU is available in the WPI MakerSpace, it was able to be printed very quickly and easily, making this material highly time effective and easily manufactured. The cost was also very low, with a price of only \$0.10 per gram.

Muscles

We selected Formlabs Elastic to represent the muscles in the model. In the literature, we found the elastic modulus of muscles to be very low, only around 0.01 to 0.08 MPa (see table 6). None of the materials that we tested were within this range. The Formlabs Elastic had an elastic modulus of approximately 8-14 MPa and the Flexible had an elastic modulus of 2-5 MPa. Although the Formlabs Flexible material was somewhat closer to the elastic modulus of natural muscles, neither materials were within the same order of magnitude. We ultimately decided to use the Formlabs Elastic for this application because, compared to the Formlabs Flexible, it had a higher fracture strength. The Formlabs Flexible failed at a tensile stress of only 3 MPa, while the Formlabs Elastic failed at about twice that stress. We also observed from working with both materials that the Flexible material cracks easier than the Elastic material. With the aim of creating a durable model, we chose to move forward with the Elastic material for the muscles. The Formlabs materials were also advantageous because they were 3D printable on campus, making them very easy to manufacture. The time and cost of manufacturing with the material was also satisfactory and the cost was well within our budget (costing about \$20-30 per cubic inch).

Ligaments

For the acromioclavicular (AC) ligament, we decided to use the same materials and construction method as the previous team. We used a braided fishing line to connect the joint and

then secured the joint with KT tape. We chose to use this method because the attachment worked well in the previous iteration of the model and we did not identify a need to change it.

For the glenohumeral ligament, we ultimately decided to use rubber exercise bands. We had originally decided to use the Formlabs Flexible material, due to it having a similar elastic modulus to ligaments. However, we found that the Formlabs Flexible material was not pliable enough and would have impeded the motion of the shoulder if used as a ligament material. Therefore we re-evaluated our other options and decided to use rubber exercise bands. The rubber bands had a similar material property to ligaments, being viscoelastic and having comparable elastic moduli (Fuentes, 2019). The rubber exercise bands were also very low cost, readily available, and easy to work with. Each band came as a sheet of rubber, which we were easily able to cut to our desired shape and size with scissors. Also, since the exercise bands came in a pack with various resistances, we were able to select the resistance level that provided sufficient support to the joint without impeding the movement of the shoulder.

3.1.3 Attachment Methods

After selecting materials to replicate the muscles and tendons, we evaluated attachment methods. The tendons, made from TPU, needed to be attached to both the PLA bone and the Formlabs Flexible muscle. Because of this, attachments were separated into two categories: bone to tendon (PLA to TPU) and tendon to muscle (TPU to Formlabs Elastic). Each attachment method was evaluated based on biomechanical accuracy, durability, manufacturability, time, cost, and maintenance in order to determine which method was the best to use.

For bone to tendon attachments, we considered welding, screws and heat sets, and adhesives. For each method, we used a spare PLA scapula and spare TPU prints that had previously been used in our tensile testing. The prints were 2 mm in thickness and about 20 mm in width, which was similar to the size we expected our attachments to be. We then tested the flexibility, strength, and durability of each bone to tendon attachment method by hand pulling on the TPU. We found that the screws and heat sets were the best option for bone-to-tendon attachments because they were able to hold the TPU close to the bone.. This attachment method would more accurately replicate the force vectors and resemble the enthesis. It was also easy to manufacture and maintain because screw and heat sets allowed for the tendon material to be

removed and replaced if desired. This quality was particularly desirable because if another iteration were to be made there would not be any permanent attachments that would limit the ability to make alterations. The downside was that the screw would create a stress concentration at the attachment point.

For tendon-to-muscle attachments, we tested nuts and bolts, sewing, suturing, and KT tape. We attached the spare dog-bone samples of TPU and Flexible Formlabs using the different methods in order to test them. After attaching them together, we pulled on the TPU and Formlabs Flexible to check for security, sturdiness, durability and any fractures that may occur. We found that suturing the elastic and TPU together was the best option because it distributed the force across many smaller holes as opposed to a few large holes. It was also a more biologically accurate attachment since sutures are used to repair tendons and thus are designed to have similar properties and distribute stresses throughout the connection point in a way that won't damage the tendons. We found that puncturing the Formlabs Flexible with the needle tended to crack the material, so we decided to add pre-made small holes to the muscle and tendon designs to prevent this cracking. This not only helped to prevent cracking, but it also made suturing easier. Appendix 9.5 shows the decision matrix for both bone-to-tendon and tendon-to-bone attachment methods with additional explanations.

After deciding to move forward with suturing, we considered the different types of suture materials and their sizes. We found that braided sutures are stronger and more similar to the fibrous structure of soft tissues compared to monofilament sutures. Since we wanted to prioritize durability in our model, we selected the braided sutures, which were available in both polyester and silk. For suture sizes, we decided to use sizes between 2-5 since these are typically used for tendon repair and we would be using them for tendon-to-muscle attachments (Oxford Medical Education, 2016).

3.1.4 Motor Location and Function

Relocate Deltoid and Supraspinatus Motors

In order to decrease the weight on the humerus caused by the original motor placements, we decided to remove the deltoid and supraspinatus motors from the humerus and place them on

the backboard of the rig. We performed calculations to quantify the force reduction from relocating the motors. The figure below shows an updated free body diagram (FBD) of the humerus with the motors removed and the table below describes the variables in the FBD.

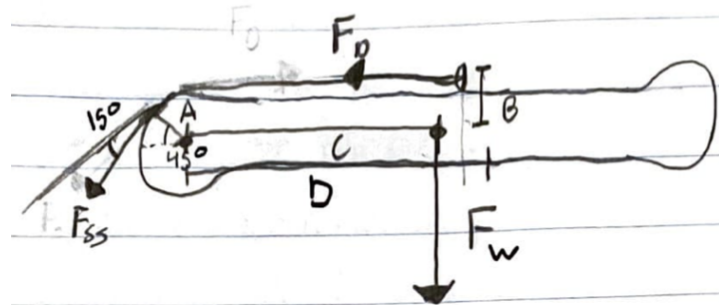


Figure 30: Free body diagram of forces on the humerus with new motor placement

Table 10: Variable descriptions for free body diagram (Deane et al, 2022)

Variable	Description	Value when humerus is at 90 degrees abduction with new motor placement
A	Distance from supraspinatus insertion point to center of rotation of the humeral head	1 in
B	Distance from the central axis of the humerus to the axis to the line of action of the deltoid	1 in
C	Distance from the center of rotation of the humeral head to the center of mass of the humerus	6 in
D	Distance from the center of rotation of the humeral head to the location of the motors (previous model) or attachment point of the deltoid muscle (new motor placement)	4 in
Fw	The weight of the 3D printed humerus	0.547 lb
Fss	Force of the supraspinatus at 90 degrees abduction	0 lb
Fm	Weight of two Nema 17 motors	N/A
Fd	Force of the deltoid at 90 degrees abduction	

One major assumption that we made when performing the following calculations was to neglect friction. In reality, there are many points of friction in the model, including friction in the joints and on the muscles, which would likely increase forces. We decided to neglect these forces for the purpose of simplifying our calculations. We also lubricated the model where necessary to minimize friction forces. Another major assumption that we made was to assume the supraspinatus muscle force is zero when the humerus is at 90 degrees of abduction. In reality, the

supraspinatus likely produces some force on the humerus, however since the deltoid is the main abducting force at this phase we assumed the supraspinatus force would be negligible.

First, we calculated the force required by the deltoid when the humerus had the two motors attached. Based on the free body diagram, we wrote an equation for the sum of the moments about the center of the humeral head. The sum of these moments must equal zero because when the humerus is at 90 degrees of abduction, it is at rest and thus has no angular acceleration. The moment equation for the humerus system would be as follows:

$$\Sigma M = F_{SS} \cdot A + F_D \cdot B - F_m \cdot D - F_w \cdot C = 0$$

Solving for F_D gives the following

$$F_D = \frac{-F_{SS} \cdot A + F_m \cdot D + F_w \cdot C}{B}$$

By inputting the values from table 10, we can arrive at a value for the force of the deltoid:

$$F_D = \frac{(0 \text{ lb}) \cdot (1 \text{ in}) + 2 \cdot (0.88 \text{ lb}) \cdot (5 \text{ in}) + (0.547 \text{ lb}) \cdot (6 \text{ in})}{1 \text{ in}}$$

$$F_D = 12.08 \text{ lb}$$

Next, we will calculate the force required by the deltoid when the motors were not attached to the humerus. When the $F_m \cdot D$ term is removed from the formula, the equation for F_D simplifies to the following:

$$F_D = \frac{-F_{SS} \cdot A + F_w \cdot C}{B}$$

Then, the values of each variable can be input to find what the new force required by the deltoid would be:

$$F_D = \frac{(0 \text{ lb})(1 \text{ in}) + (0.547 \text{ lb})(6 \text{ in})}{1 \text{ in}}$$

$$F_D = 3.28 \text{ lb}$$

These calculations showed that, by removing the weight of the two motors from the humerus, we actually reduced the estimated force required by the deltoid by more than 70%.

Create anatomically accurate force vectors

We considered a few different options for motor placement of the deltoid and scapula including support structures, attaching the motors to the rig and using hooks, and a bowden cable. We ruled out support structures because we did not want to obstruct future ranges of motion. In deciding between hooks or bowden cables, we chose bowden cables because the cable has the benefit of creating an opposite and equal force on the bone. Hooks would have allowed us to guide the muscle along the correct line of action, but would have provided additional forces and moved bones unintentionally. The bowden cable prevented this by ensuring the forces from the supraspinatus and deltoid were applied correctly. Additionally, the flexibility of the bowden cable allowed us to place the supraspinatus and deltoid motor wherever we needed since it directs where the force is applied. Because of these reasons, we moved forward with the bowden cable for our supraspinatus and deltoid motor relocation. Within our model, the bowden cables were originally placed on the supraspinatus and the deltoid. The inside cable, made of TPU, was secured on the humerus and led to the scapula where the outside cable was attached. The other end of the outside cable was attached and secured near the motor while the inside cable was wound around the motor. This resulted in the TPU muscle compressing, which is biologically accurate. Since the outside cable could not move while the inside cable (TPU) pulled the scapula and humerus towards it, the outside cable would provide a force in the opposite direction to that of the TPU. This resulted in forces acting on both the scapula and the humerus, as discussed in Section 2.2, The deltoid bowden cable was eventually removed due to torque complications with the deltoid motor.

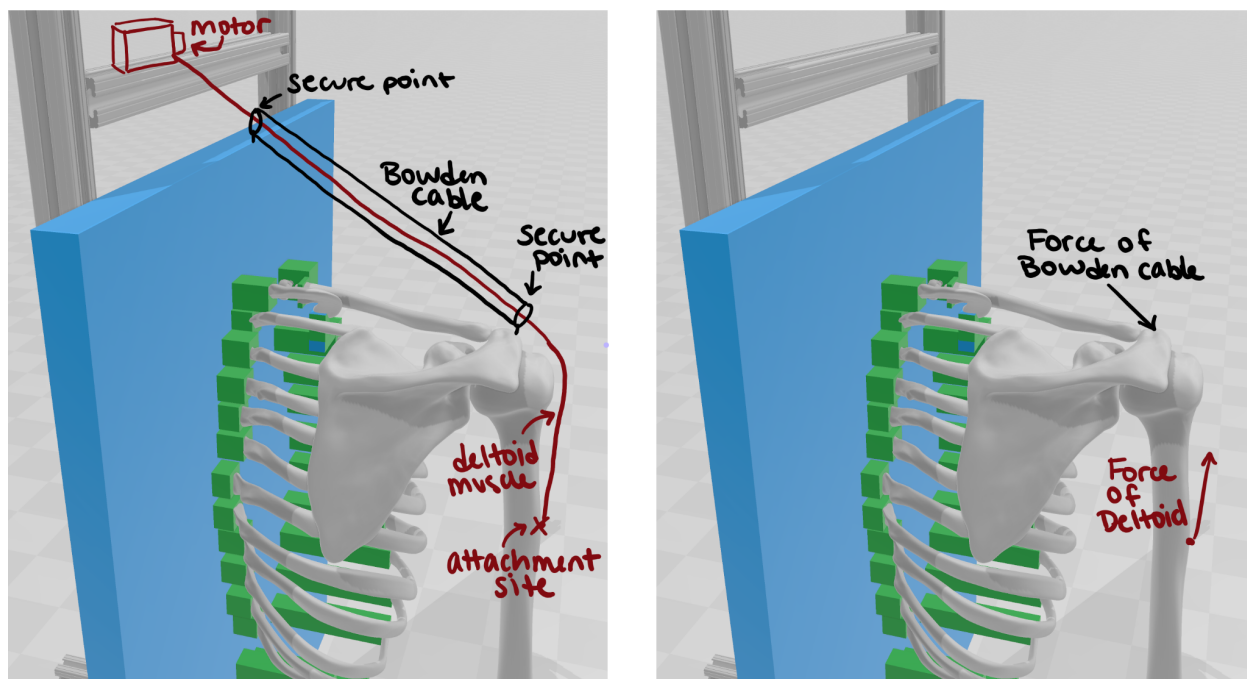


Figure 31: (left) Diagram showing bowden cable on the model, (right) force vectors of the deltoid muscle and bowden cable on the humerus and scapula respectively.



Figure 32: Bowden cable at use in the model on the supraspinatus muscle.

Circuit Building and Motor Coding

After determining the placement of the motors, we built the circuit and coded the system in order to achieve scapulohumeral rotation. We followed the previous team's circuit set up to create the circuit using an Arduino Uno and five A4988 microprocessors to communicate with the five stepper motors. Additionally we added a second power source so that the deltoid muscle had its own power, The circuit can be seen below in figure 33.

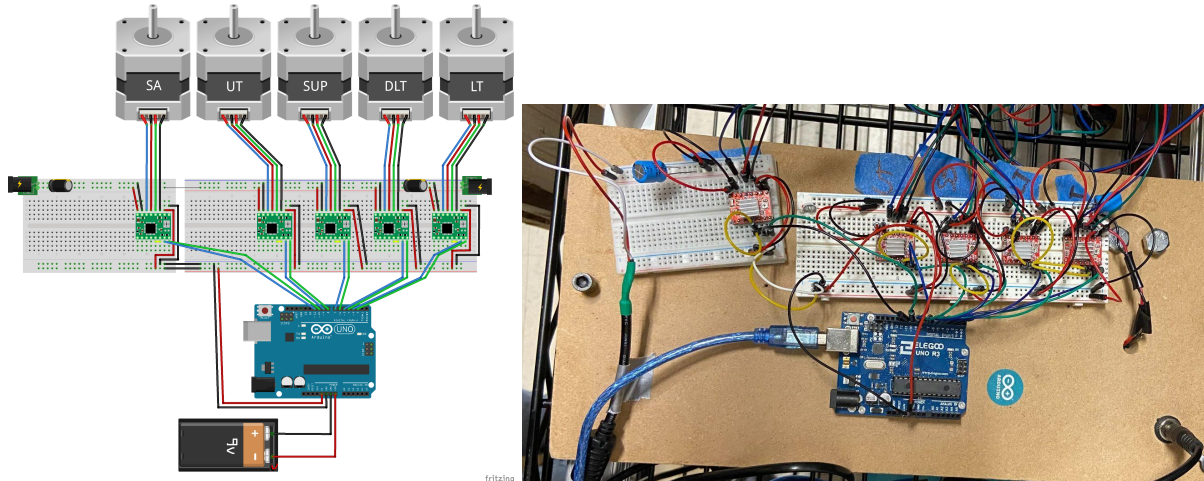


Figure 33: Circuit with arduino, microprocessors, and motors diagram (left) and set up (right)

We separated the movement of abduction into four motions: 0-15 degrees, 15-30 degrees, 30-60 degrees, and 60-90 degrees. The motors were adjusted so that the muscles were taut and held the scapula and humerus at their resting positions. The starting position was defined as the humerus and scapula both being at 0 degrees of rotation. The humerus and scapula were then rotated to their respective degree of rotation for each motion: the humerus to 15, 30, 60, and 90 degrees and the scapula to 0, 0, 15, and 30 degrees, respectively. While holding the humerus and scapula in place, the muscles were pulled taut and the changes in length were marked. The length from the new mark to the starting mark was measured in millimeters, marking the distance that the motor would need to pull. These lengths were recorded in Appendix 9.6. The motors were coded based on the number of steps that each motor needed to pull to create the proper change in length for each stage of abduction. The distances were converted to motor steps using the following equation:

$$\frac{\pi * D_{Spool}}{Steps/Revolution} * Distance = Steps$$

The calculated steps of each muscle for each motion was taken and put into the code, which was modified from the previous team. The calculated number of steps were used as a guideline for the code and the code was updated during troubleshooting depending on if a muscle needed to pull more or less. The most important update in the code was changing each motor's speed in between each stage of abduction. This allowed for the motors to complete the stages at the same time. The full code can be seen in Appendix 9.7. This code communicated each abduction motion to the motors, moving all five motors simultaneously.

3.2 Testing Methods

3.2.1 Model Function Goals

By improving the motor location and function, materials for soft tissues, and attachment methods used in the model, we aimed to achieve more anatomically accurate movement in the model. Our criteria for more anatomically accurate movement is outlined below:

1. Consistently abduct the humerus from zero degrees to 90 degrees
2. Consistently return the humerus and scapula to their original starting positions after each abduction cycle
3. Achieve an accurate scapulohumeral rhythm in the model, meaning that:
 - a. The scapula remains at rest until 30 degrees of humeral abduction
 - b. Between 30 to 90 degrees of humeral abduction the scapula upwardly rotates one degree for each two degrees of humeral abduction
 - c. When the humerus is at 90 degrees abduction, the scapula has a posterior tilt of 7.5 degrees
 - d. When the humerus is at 90 degrees of abduction, the scapula has an external rotation of 3.3 degrees

3.2.2 Movement Tracking Dots

In order to evaluate the movement goals of our model, we used a procedure similar to that of the previous team. First, to help track the movement accurately, we placed seven circular

stickers on the scapula and two circular stickers on the humerus. Three circular stickers were placed on the posterior (back) of the scapula to track its upward rotation, two circular stickers were placed on the lateral (side) of the scapula to track its posterior tilting, and two circular stickers were placed on the superior (top) of the scapula to track its external rotation. Two circular stickers were placed on the humerus to track its abduction angle. The figure below shows an illustration of the scapula with red dots to represent where the stickers were placed:

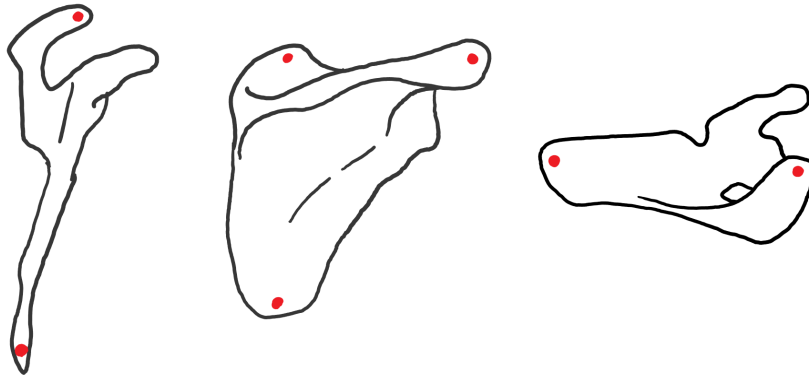


Figure 34: Illustration showing location of stickers on the scapula. Left drawing shows the side view, middle drawing shows the back view, and right drawing shows the top view.

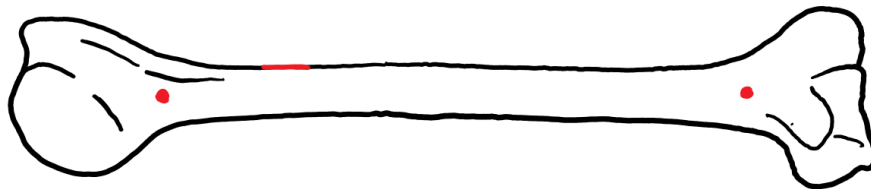


Figure 35: Illustration showing location of stickers on the humerus.

3.2.3 Testing Procedure

To begin our testing procedure, we set up three different smartphone cameras to capture the three different planes of movement. We captured a superior (or top) view, a posterior (or back) view, and a lateral (or side) view of the system. For the superior view, we attached an aluminum extrusion nine inches above the backboard of the model. We then rested a smartphone on the aluminum extrusion so that the camera pointed directly downward over the model. For the

posterior and lateral views, we utilized two 40-inch-tall tripods. To capture the lateral view, we placed one tripod about 30-inches away from the model and parallel to the backboard of the model. We then adjusted the smartphone so that the model was in the center of the frame. Similarly, to capture the posterior view, we placed the other tripod about 45-inches away from the model and perpendicular to the backboard. We adjusted the smartphone so that the scapula and humerus were completely visible and in the center of the frame.

For each trial, we programmed the model to abduct over a 35 second period, pause for 5 seconds, and then adduct over a 35 second period back to the resting position. For simplicity, adduction was modeled as abduction in reverse rather than its own motion with a different set of muscles. Between trials, we manually reset the model to the resting position. This manual reset was necessary because each trial would end with slack in the deltoid muscle, causing subsequent trials to be less accurate. To maximize the performance of the model, we manually tightened the deltoid motor to return it to the starting position. We ran three trials, recording video of each trial in the three dimensions previously described (superior, posterior, and lateral). We used Kinovea, a video annotation tool commonly used in sports analysis, to find the angle of rotation of the scapula and humerus at multiple points over the abduction cycle. Using the dots on the scapula as a measurement guide, we were able to measure the degrees of upward rotation, posterior tilt, and external rotation of the scapula at each interval of abduction. We used the “measure angle from vertical” tool in Kinovea to track the angles (see figure below). The starting angle from the vertical was considered the resting position, and the change in angle of the humerus and scapula were measured relative to the resting position. A measurement was taken every two degrees of humeral abduction until the maximum abduction was reached. The exact moment of each two degree mark was determined by analyzing the video frame by frame. We also quantified the maximum abduction achieved in each movement, as well as how closely the model returned to the resting position. We used this data to compare how well our model achieved our motion goals.



Figure 36: The videos of the abduction movement were analyzed using the “measure angle from vertical” tool in Kinovea.

4. Results

After recording several cycles of abduction, we decided to use the first three trials that we performed because the deltoid motor began to burn out. The first three trials were the most indicative of the accuracy the model is able to achieve with functional motors. The model was evaluated based on how well it was able to achieve our original three goals: abduct to 90 degrees, return to 0 degrees, and accurate scapulohumeral rhythm.

4.1 Abducts to 90 degrees

To measure how well our model met our goal of consistently abducting to 90 degrees, we located the moment in the recorded videos where the humerus reached its maximum abduction. The resulting maximum abduction was 43.5, 38.8, and 40.8 during trials one, two, and three respectively. The average maximum abduction was 41.03 degrees with a standard deviation of 2.34 degrees.

The figures below demonstrate how the raw measurements were taken for humerus and scapula rotation. First, the angles of elevation for each bone were taken with respect to the vertical axis (see figure 37). Then, the initial position was subtracted from these measurements to arrive at a change in angle. The initial position can be seen in figure 38 below. This change in angle is what we used as the measurement of humeral abduction and scapular rotation respectively.

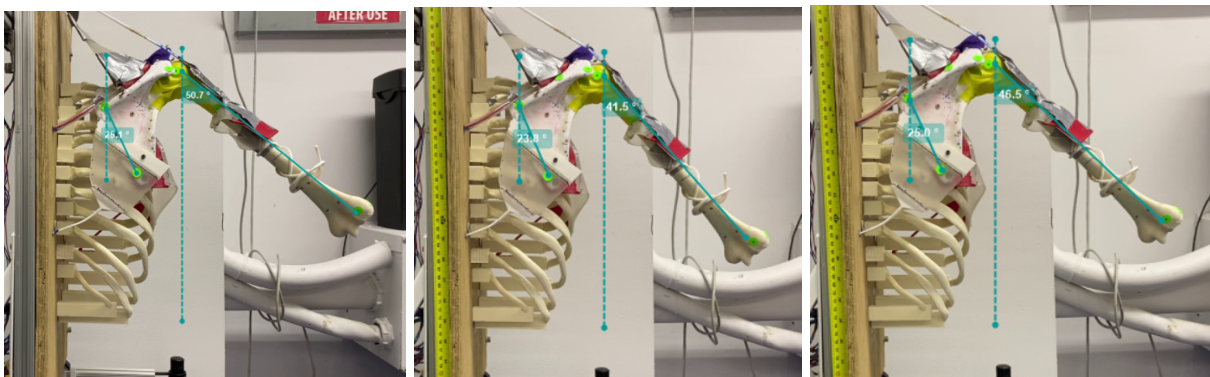


Figure 37: Maximum abduction of trials one, two, and three.

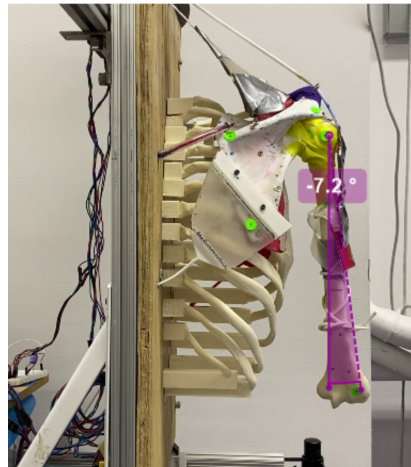


Figure 38: Initial position of humerus for trial one

4.2 Returns to 0 degrees

We next determined how well our model returned to its initial position after completing each abduction cycle. We located the moment in the recorded videos where the humerus returned to rest after each trial. We determined the position of the tracking dots when the humerus was at rest and compared these positions to the ideal resting position of the humerus. It was determined that the humerus did return to the resting position; however, there was slack in the deltoid muscle. This slack in the deltoid muscle caused future cycles to be less accurate, so we manually reset the model to its resting position between trials.

4.3 Accurate Scapulohumeral Rhythm

4.3.1 Back View

To compare the model's achieved scapulohumeral rhythm to the ideal scapulohumeral rhythm in the back view, we took measurements of scapula rotation for every two degrees of humeral abduction until maximum abduction (full data table can be found in appendix 9.9). The graph below shows the measured (blue) and ideal (orange) scapula rotation as a function of humeral abduction. It can be seen that the scapula remains at rest until 20 degrees of abduction. Ideally, the scapula would remain at rest until 30 degrees of abduction, so our model achieved accuracy to within 33.33% of this goal. Once the scapula starts rotating, it rotates up to 12

degrees in the next 20 degrees of humeral abduction. This ratio of 1 degree of scapula rotation to 1.67 degrees of humeral abduction is within 16.5% of the ideal value of 1 degree of scapula rotation to 2 degrees of humeral abduction.

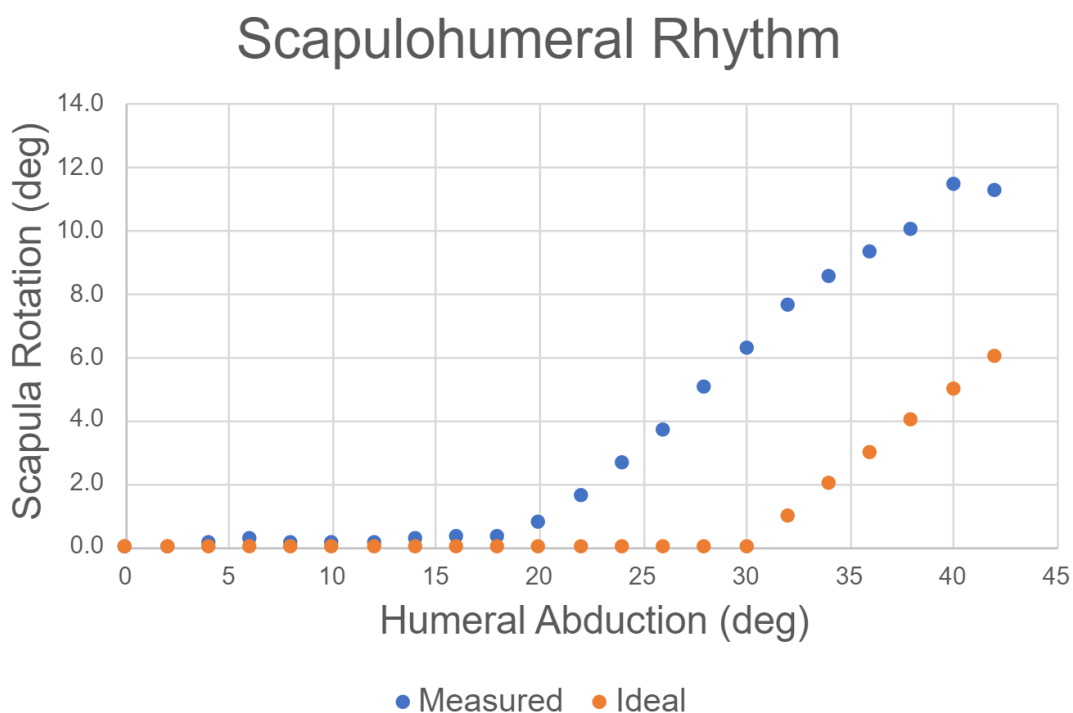


Figure 39: A graph portraying measured (blue) and ideal (orange) scapula rotation as a function of humeral abduction.

4.3.2 Top View

The top view of the scapula was used to determine the internal/external rotation of the scapula with respect to humerus abduction (see graph below). We found that the scapula in the model experiences external rotation when it should be experiencing internal rotation during the abduction process.

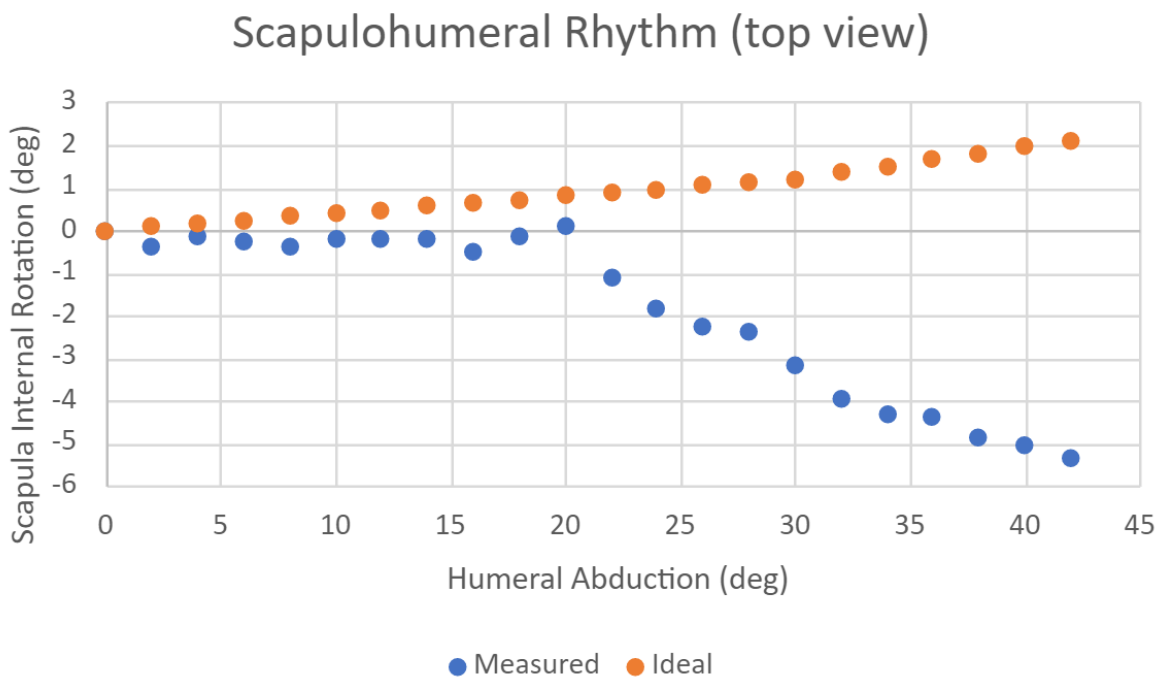


Figure 40: Scapula internal rotation as a function of humerus abduction. The scapula in the model rotates externally during abduction rather than internally.

4.3.3 Side View

In reviewing our video footage, we observed that the scapula was blocked by the humerus as the humerus deviated from the plane of motion. Rather than tracking scapulohumeral rhythm via this view, we tracked humeral deviation. We took measurements of humeral deviation for every two degrees of humerus abduction and graphed humerus deviation as a function of humerus abduction (see figure below). It was found that the humerus deviates about one degree for every two degrees of abduction.

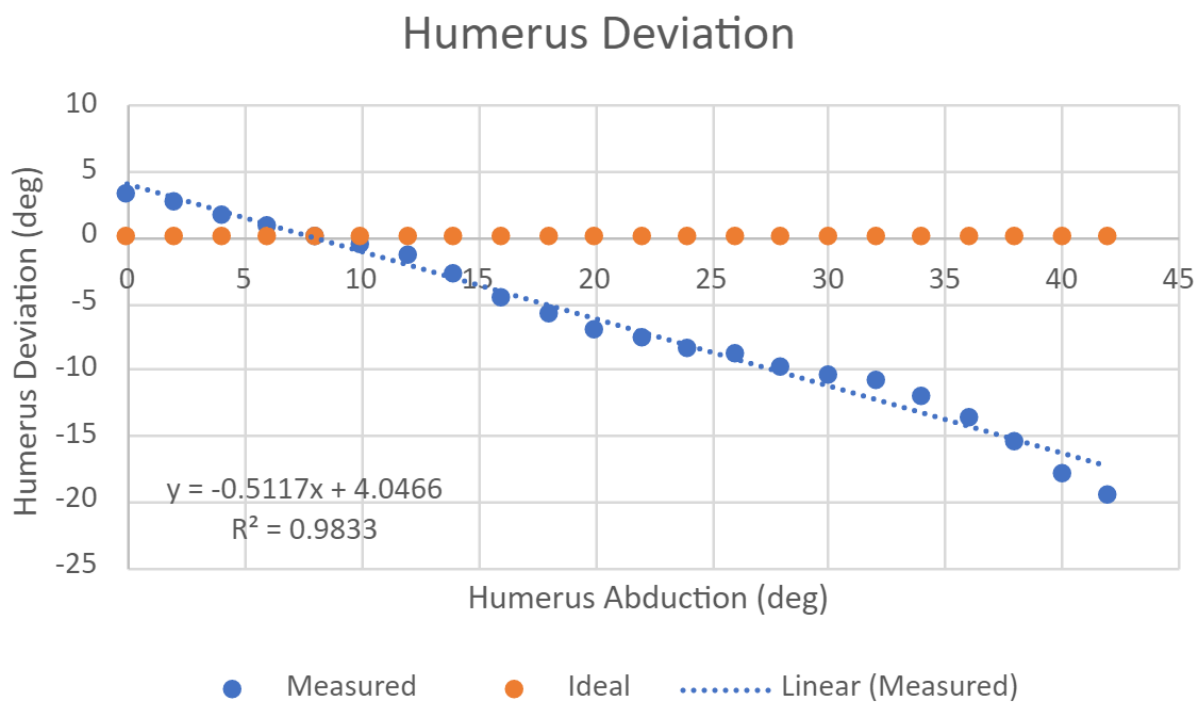


Figure 41: Humerus deviation as a function of abduction.

5. Discussion

After reviewing the results, we were able to determine our successes and shortcomings.

5.1 Motor Location and Function

In terms of motor location and function, we were able to remove the deltoid and supraspinatus motors from the arm of the model, reducing the weight of the humerus. We were also successfully able to create biologically accurate force vectors by relocating the muscles to pull in the appropriate directions. Additionally, we were able to successfully measure the change in length of the muscles and convert the measurements to steps to communicate the needed change through the arduino code. A shortcoming of this section was the function of the deltoid motor. While it was successfully repositioned to create the proper force vector, it was not able to complete its rotation during the abduction cycle. The deltoid was only successful at pulling the humerus from zero to 60 degrees. However, from 60-90 degrees, the motor would slip and not pull the deltoid any further. We observed that the deltoid could complete the full rotation when it was running by itself, but not while the other motors were also running. After conducting extensive troubleshooting, we propose that the cause of this was likely too much torque on the motor and lack of feedback loops and proportional integral derivative control in the code. Additionally, we noticed the deltoid motor heated up after several abduction trials. Overheating can reduce the amount of torque a stepper motor can apply, which might have contributed to the decrease of the deltoid function over time. In terms of the code, the lack of feedback loops and proportional integral derivative control may have resulted in the code becoming stuck or miscommunicating with the motors, resulting in the deltoid not moving correctly. Feedback loops would indicate how the motor was moving and proportional integral derivative control would have adjusted the motors to guarantee they were moving in sync with each other.

5.2 Material Selection

Material selection of tendons, muscles, and ligaments was generally successful. The materials selected were able to be incorporated into the physical model. Both the TPU and Formablabs Elastic were able to last through testing without deformation, ensuring the longevity of the model for the duration of this project. They had yield strengths higher than the anticipated

stresses as well. The TPU and Formlabs Elastic also had low friction and were sufficiently pliable, so they were able to easily slide and form to the bones when necessary. This and the fact that they did not deform preserved functionality of the model.

In terms of mimicking the biological material with comparable material properties, we were successful in some areas but fell short in others. The rubber exercise bands mimicked the ligaments well as they had an elastic modulus range of 2.9-6.5 MPa and biological ligaments had an elastic modulus of 3.4 to 6.3 MPa. Similarly, the TPU mimicked the tendons as the TPU had an elastic modulus of 437 MPa, which fell in the range of tendon elastic modulus: 217.7 to 592.4. While the elastic exercise band and TPU had accurate elastic moduli for the biological material they were mimicking, the Formlabs Elastic fell short in this category. The Formlabs Elastic had a modulus of 8 to 14 MPa while muscles, which the Formlab Elastic mimicked, had an elastic modulus of 0.017 to 0.063 MPa.

Additionally, another part of this goal was for the materials that were mimicking the tendon and muscles to have similar stress strain curves to that of the natural tendons and ligaments. This was unsuccessful because, although the stress strain curves had both linear and non linear regions, the TPU lacked the toe region that natural tendons have before the linear region. The shortcomings for material properties were largely due to time and manufacturing constraints. With more time and access to different manufacturing, a more extensive material selection could have been explored.

5.3 Attachment Methods

The attachment methods successfully placed the tendon and bone closer together and improved the bone to tendon and tendon to bone transitions. The tendon-to-bone attachments were able to transmit the forces of the muscles to the bone in accurate directions. Additionally the screw and heat set tendon and bone attachment was a secure attachment and did not break. This attachment was also better able to better mimic the enthesis region in the way that it brought the tendon closer to the bone. While this was improved from the previous iteration, it did not exactly replicate the enthesis. Improvements on replicating the enthesis could involve embedding the tendon into the bone. This method was not explored in this iteration in order to preserve the bone structure of the model for future teams.

A shortcoming in our attachment methods were the tendon-to-muscle attachments. While the attachment better replicated the transition region of tendon to muscles by overlapping the TPU and formlabs elastic, the suturing caused stress concentrations resulting in breakage of tendon-to-muscle attachments. Initially, the suturing attachment method appeared strong and was able to resist breaking when force was applied. However, after several cycles of force application, tearing began to occur. This failure was potentially caused by the stress concentrations from the small holes on the muscle and tendons. Future iterations should consider fatigue testing on both the attachment methods and the materials in order to determine how many cycles the model can withstand.

5.4 Movement

Improvements for the accuracy of the abduction cycle were also made. We were able to successfully delay the scapula rotation until 20 degrees of humeral rotation, where the previous iteration did not delay at all. The maximum humeral rotation achieved was 46.6 degrees, which is less than the previous team achieved, but still within 50% of our goal. Additionally, the scapula humeral rotation had a ratio of 1:1.67 up until maximum abduction which was an improvement from the previous team's iteration. The scapula and humerus were also able to return to rest with slack in the deltoid. As stated before, the shortcomings of this movement is likely related to the deltoid motor's inability to complete its cycle. An improvement of the deltoid motor would help with the delay of scapula rotation until 30 degrees of humeral rotation and improve the scapulohumeral rotation as well potentially abduct the humerus to 90 degrees. The scapula over-rotated on the side and externally rotated instead of internally when compared to the ideal scapula rotation. This is potentially due to the lower trapezius pulling too much and the serratus anterior pulling too little. A way to fix this would be to take more precise measurements while focusing on the scapula from several different angles and by adjusting the number of steps and speed of the motor when deviation is recognized.

6. Conclusions and Recommendations

The goal of this project was to improve upon the previous team's iteration by focusing on soft tissue materials, attachment methods, and motor placement. To accomplish this, we selected materials which possessed similar elastic moduli to biological tendons, muscles, and ligaments. We also created attachments that more closely replicated the transition from bone to tendon to muscle. Lastly, we relocated the motors to reduce weight on the humerus and produce anatomically accurate motion vectors from each muscle. We then revised the motor code to produce our desired motion. Although our movement goals were not fully realized, the modifications we made to the model did result in some measurable improvements and achievements. For instance, we were able to achieve partial abduction of the humerus, improve the scapulohumeral rhythm, and improve the robustness of the soft tissues.

Despite what we were able to achieve, there are several areas of improvement, and we hope that future teams continue to develop this model. In the future, a more extensive exploration of muscle and tendon materials could be conducted in order to find a material with a stress-strain curve that more closely matches biological soft tissues. Our material investigation was limited and, while we were able to find materials which possessed similar elastic moduli to soft tissues, we did not find any which possessed the same uniquely shaped stress-strain curve. Finding materials which are able to mimic the particular regions of a soft tissue stress-strain curve would be beneficial since these unique material properties of these tissues play an important role in the biomechanics of the human body. Furthermore, more rigorous testing of attachment methods could also be performed in order to ensure longevity of the model. While we took a great amount of care when selecting attachment methods, we found that the repeated movement of the model caused these attachment points to tear. Conducting tensile testing and fatigue testing of attachment methods may help to improve the durability of attachments. We also think that more investigation could be done to discover how to properly actuate the deltoid muscle so that the humerus can achieve a full 90 degrees of abduction. In our time working with the model, we identified the deltoid muscle as a limiting factor in achieving our full goal for abduction. Therefore, examining this muscle more closely may be valuable. Another next step for the future may be to continue developing more ranges of motion, such as flexion and

extension (i.e. moving the arm in front of and behind the body). This could be done through the addition of new muscles and modifications to the code.

With an improved range of motion as well as more accurate material attachments, this model has the potential to be used as an education and research tool. The model could be used to accurately replicate shoulder injuries for the purposes of studying the biomechanics and injury mechanisms of the shoulder. It may also be used to educate students of medicine and other related fields in the complex functions and motions of the human shoulder.

7. Broader Impacts

7.1 Engineering Ethics

When completing our project, we strived to meet the engineering code of ethics set forth by the American Society of Mechanical Engineering. We paid close attention to the fundamental principles established in this code and took great care to uphold them. We used our expertise as mechanical engineers to create this model so that in the future it could be used to benefit the health and wellbeing of people with shoulder injuries. Throughout our report we strived to be as truthful and objective as possible in order to preserve the integrity of our work. We hope that our accomplishments within this project reflect well on ourselves and on the engineering field as a whole.

Since this project was a continuation of the shoulder model created the year prior, we took great care to respect the progress made by the previous team. We respected this team's right to the intellectual property and communicated with them clearly and openly to avoid violating those IP rights. As we worked off of the previous model iteration, we strived to improve the model by conducting our own research and adding our own modifications.

In completing this project, we sought to create the best quality model we could. We conducted extensive research from reputable sources and conducted business with trustworthy vendors. We utilized our engineering expertise and knowledge of biomechanics to create a model that was as accurate as possible. We also were careful to consider the broader impacts of our project, including social and global impacts, environmental impacts, and economic impacts. These impacts are discussed further throughout this chapter.

7.2 Social and Global Impact

Further developments of this model have the potential to be used for injury prevention and repairs, medical education, and medical device testing. An anatomically accurate shoulder model that is able to perform abduction, adduction, flexion, and extension would be able to simulate shoulder injuries and contribute to furthering research on injury prevention. This could help people who are prone to shoulder injuries such as athletes, people with arthritis, and middle

aged and older adults. Additionally, research regarding repair and recovery of shoulder injuries could be performed on the model. This could contribute to better recovery methods that could lead to shorter recovery times or increased range of motion post injury. Both injury prevention and repair can be advanced by the shoulder model which may lead to decreased medical costs and recovery time of patients. For the medical device industry, medical devices can be tested on the model before moving into human testing. This would allow for medical device companies to adjust their device to the motion of the shoulder and any shoulder injury before moving into human testing potentially saving time and device iterations after human testing. Finally, the model could be used in medical education to better display the complexities of the human shoulder and how the muscles and ligaments contribute to the movement of the shoulder.

7.3 Environmental Impact

The materials used in this model include Polylactic Acid (PLA), KT Tape, Formlabs Elastic 50A, Formlabs Flexible 80A, and Thermoplastic Polyurethane (TPU). The previous team chose to use PLA and KT tape. PLA is biodegradable and takes only 12 weeks to decompose. While KT tape is synthetic and a waste material, it is able to be used long term in our model, so it will not contribute too much waste. The materials that we selected are Formlabs Elastic 50A and TPU. Formlabs Elastic 50A is an elastomeric resin material and not biodegradable; however, it is durable. When choosing materials for our model, we prioritized durability so that they can be used long term. TPU is also not biodegradable, but it is both durable and reusable. If the TPU on the model needs to be altered or replaced, it can be melted and reused to make different parts. In addition to these materials, we also added more aluminum extrusions to mount our motors in a similar way to the previous team. We gained these materials by using scrap materials from previous projects, so few new materials were needed. In terms of manufacturing, we used 3D printing, which is better for the environment because it generates less material waste and requires less energy compared to traditional plastic manufacturing.

7.4 Economic Impact

The cost of the model is relatively low. The bones, muscles, and tendons were made from PLA, Formlabs Elastic, and TPU respectively. All of these materials were relatively inexpensive and accessible using 3D printing. The stepper motors, rubber exercise band, aluminum extrusion,

plywood, screws, heat sets, Arudino and circuit board also contributed to the cost of the model. These components are also inexpensive and accessible through vendors such as Amazon and Home Depot.

8. Citations

- Aghaei, A., Bochud, N., Rosi, G., & Naili, S. (2021). Assessing the effective elastic properties of the tendon-to-bone insertion: a multiscale modeling approach. *Biomechanics and Modeling in Mechanobiology*, 20(2), 433-448.
- Anatomical Terminology*. Anatomical Terminology | SEER Training. (n.d.). Retrieved October 13, 2022, from <https://training.seer.cancer.gov/anatomy/body/terminology.html>
- Anatomical Terms of Movement*. TeachMeAnatomy. (n.d.). Retrieved October 13, 2022, from <https://teachmeanatomy.info/the-basics/anatomical-terminology/terms-of-movement/>
- Anatomy Language: Part II*. NolanLee.com. (n.d.). Retrieved October 13, 2022, from <http://www.nolanlee.com/blog/anatomy-language-part-ii>
- ASTM Standard D638, 2022, “Standard Test Method for Tensile Properties of Plastics,” ASTM International, West Conshohocken, PA, www.astm.org
- Avin KG, Bloomfield SA, Gross TS, Warden SJ. Biomechanical aspects of the muscle-bone interaction. *Curr Osteoporos Rep*. 2015 Feb;13(1):1-8. doi: 10.1007/s11914-014-0244-x. PMID: 25515697; PMCID: PMC4306629.
- Benjamin, M., Toumi, H., Ralphs, J. R., Bydder, G., Best, T. M., & Milz, S. (2006). Where tendons and ligaments meet bone: attachment sites (‘entheses’) in relation to exercise and/or mechanical load. *Journal of anatomy*, 208(4), 471-490.
- Bey, Hunter, S. A., Kilambi, N., Butler, D. L., & Lindenfeld, T. N. (2005). Structural and mechanical properties of the glenohumeral joint posterior capsule. *Journal of Shoulder and Elbow Surgery*, 14(2), 201–206. <https://doi.org/10.1016/j.jse.2004.06.016>
- Cleveland Clinic Medical Professionals. (n.d.). *Muscle: Types of muscles, functions & common conditions*. Cleveland Clinic. Retrieved December 19, 2022, from <https://my.clevelandclinic.org/health/body/21887-muscle>
- Lamtner, B. (2022, July 13). Towards more effective tendon repair with a multi-functional biomaterial. Wyss Institute. Retrieved September 15, 2022, from <https://wyss.harvard.edu/news/towards-more-effective-tendon-repair-with-a-multi-functional-biomaterial>
- Britannica. (n.d.) *The Shoulder*. <https://www.britannica.com/science/human-muscle-system/The-shoulder>

- Deane, E., LaBlanc, D., Savage, B., Winters, S. (2022). Anatomically Accurate Motorized Shoulder Model with Scapula Movement.
- Dekker, T. J., Aman, Z. S., Peebles, L. A., Storaci, H. W., Chahla, J., Millett, P. J., & Provencher, M. T. (2020). Quantitative and qualitative analyses of the glenohumeral ligaments: An anatomic study. *The American Journal of Sports Medicine*, 48(8), 1837–1845. <https://doi.org/10.1177/0363546520917665>
- Engineering Resin: Flexible 80A*. (2020, 29 May). Formlabs. Retrieved October 12, 2022, from <https://formlabs.com/materials/flexible-elastic/>
- Formlabs. (n.d.). *What is the Melting Point of Formlabs Resins*. Formlabs Customer Support. Retrieved December 16, 2022, from <https://support.formlabs.com/s/article/What-is-the-melting-point-of-Formlabs-resins>
- Frontera, W. R., & Ochala, J. (2014). Skeletal muscle: A brief review of structure and function. *Calcified Tissue International*, 96(3), 183–195. <https://doi.org/10.1007/s00223-014-9915-y>
- Fuentes, A. D., Smith, C. J., & Shoepe, T. C. (2019). Loading Patterns of Rubber-Based Resistance Bands across Distributors. *Sports (Basel, Switzerland)*, 7(1), 21. <https://doi.org/10.3390/sports7010021>
- Hatta, T., Giambini, H., Sukegawa, K., Yamanaka, Y., Sperling, J. W., Steinmann, S. P., Itoi, E., & An, K.-N. (2016). Quantified mechanical properties of the deltoid muscle using the shear wave elastography: Potential implications for reverse shoulder arthroplasty. *PLOS ONE*, 11(5). <https://doi.org/10.1371/journal.pone.0155102>
- Irving, M. (2022, January 5). *Slug-slime-inspired biomaterial speeds repair of injured tendons*. New Atlas. Retrieved January 7, 2023, from <https://newatlas.com/medical/janus-tough-adhesive-tendon-injury/>
- Koh, Cavanaugh, J. M., Leach, J. P., & Rouhana, S. W. (2004). Mechanical Properties of the Shoulder Ligaments under Dynamic Loading. *Stapp Car Crash Journal*, 48, 125–153.
- Lam, J. H., & Bordoni, B. (2021). Anatomy, Shoulder and Upper Limb, Arm Abductor Muscles. In StatPearls [Internet]. StatPearls Publishing, from <https://www.ncbi.nlm.nih.gov/books/NBK537148/>
- Lee, Kim, D., Jang, Y., & Jin, H. (2020). Three-dimensional in vivo scapular kinematics and scapulohumeral rhythm: a comparison between active and passive motion. *Journal of Shoulder and Elbow Surgery*, 29(1), 185–194. <https://doi.org/10.1016/j.jse.2019.05.036>

- Leong, H.-T., Ng, G. Y.-fat, Leung, V. Y.-fong, & Fu, S. N. (2013). Quantitative estimation of muscle shear elastic modulus of the upper trapezius with supersonic shear imaging during arm positioning. *PLoS ONE*, 8(6). <https://doi.org/10.1371/journal.pone.0067199>
- Material Data Sheet: Elastic 50A*. (2019, 7 Jan). Formlabs. Retrieved October 12, 2022, from <https://formlabs.com/materials/flexible-elastic/>
- Mold Star 15 16 30 Technical Bulletin*. (n.d.) Reynolds Advanced Materials. Retrieved October 12, 2022 from <https://www.reynoldsam.com/product/mold-star/>
- Newsroom , S. (2001, February 24). UCLA materials scientists show way to make durable artificial tendons from improved hydrogels. UCLA Samueli School Of Engineering. Retrieved October 13, 2022, from <https://samueli.ucla.edu/ucla-materials-scientists-show-way-to-make-durable-artificial-tendons-from-improved-hydrogels/>
- Matsushashi, Hooke, A. W., Zhao, K. D., Goto, A., Sperling, J. W., Steinmann, S. P., & An, K.-N. (2014). Tensile properties of a morphologically split supraspinatus tendon. *Clinical Anatomy (New York, N.Y.)*, 27(5), 702–706. <https://doi.org/10.1002/ca.22322>
- Oxford Medical Education. (2016, April 11). *Suture sizes and suggested indications for their use*. Oxford Medical Education. Retrieved February 17, 2023, from <https://oxfordmedicaleducation.com/surgery/suture-sizes-and-suggested-indications-for-their-use/>
- Porcznik, M. (2003). Attaching tendon to bone: A new framework to improve healing. AAOS. Retrieved September 7, 2022, from <https://www.aaos.org/aaosnow/2009/mar/research/research4/>
- Schenkman, M., & Rugo de Cartaya, V. (1987). Kinesiology of the shoulder complex. *Journal of Orthopaedic & Sports Physical Therapy*, 8(9), 438-450. From <https://www.jospt.org/doi/abs/10.2519/jospt.1987.8.9.438>
- Scapulohumeral Rhythm. Physiopedia. (n.d.). Retrieved October 13, 2022, from https://www.physio-pedia.com/Scapulohumeral_Rhythm#Characteristics_.2F_Clinical_Presentation
- Schwartz, A., & Thomopoulos, S. (2013). The role of mechanobiology in the attachment of tendon to bone. In *Structural Interfaces and Attachments in Biology* (pp. 229-257). Springer, New York, NY.

- Sensini, A. & Cristofolini, L. Biofabrication of Electrospun Scaffolds for the Regeneration of Tendons and Ligaments. *Materials (Basel)*. 2018 Oct 12;11(10):1963. doi: 10.3390/ma11101963. PMID: 30322082; PMCID: PMC6213815.
- Shoulder Anatomy*. (n.d.). Lex Medicus. Retrieved on October 12, 2022, from <https://anatomy.lexmedicus.com.au/collection/shoulder>
- Singh, A. P. (n.d.) *Muscles of Shoulder Region*. Bones and Spine. <https://boneandspine.com/muscles-of-shoulder/>
- Tango: Polyjet Simulated Rubber Material*. (n.d.). Stratasys. Retrieved October 12, 2022, from <https://www.stratasys.com/en/materials/materials-catalog/polyjet-materials/tango/>
- Technical Data Sheet: Standard PLA*. (n.d.). 3-D Fuel. Retrieved October 12, 2022, from <https://www.3dfuel.com/collections/standard-pla/products/ingeo-pla-standard-black>
- Ultimaker Nylon: Technical Data Sheet*. (2022, 20 Apr). Ultimaker. Retrieved October 12, 2022, from <https://ultimaker.com/materials/nylon>
- Ultimaker TPU 95A: Technical Data Sheet*. (2022, 29 Apr). Ultimaker. Retrieved October 12, 2022, from <https://ultimaker.com/materials/tpu-95a>
- Wang, J.H., Guo, Q., Li, B. (2012) Tendon biomechanics and mechanobiology--a minireview of basic concepts and recent advancements. *J Hand Ther*. 2012 Apr-Jun;25(2):133-40; quiz 141. doi: 10.1016/j.jht.2011.07.004. Epub 2011 Sep 17. PMID: 21925835; PMCID: PMC3244520.
- Yamaura, K., Mifune, Y., Inui, A., Nishimoto, H., Kataoka, T., Kurosawa, T., Mukohara, S., Niikura, T., Kokubu, T., & Kuroda, R. (2021). Sequential changes in posterior shoulder muscle elasticity after throwing as assessed via ultrasound shear wave elastography. *Orthopaedic Journal of Sports Medicine*, 9(8), 232596712110213. <https://doi.org/10.1177/23259671211021362>

9. Appendices

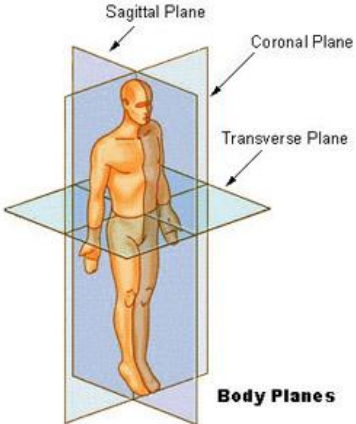
9.1 Anatomical Terminology

Table 11: Anatomical Terminology (Anatomical Terminology, n.d.)

Term	Definition
Superior	Toward the head
Inferior	Away from the head
Medial	Towards the midline of the body
Lateral	Away from the midline of the body
Anterior	Front of the body
Posterior	Back of the body
Flexion	Movement that decreases the angle between two body parts
Extension	Movement that increases the angle between two body parts
Adduction	Movement away from the midline
Abduction	Movement towards the midline
Internal Rotation/Medial Rotation	Rotational movement towards midline
Lateral Rotation	Rotational movement away from midline
Elevation	Movement in superior direction
Depression	Movement in inferior direction
Protraction	Movement towards the front of the body
Axial Skeleton	Central axis of the skeleton including the bone, skull, laryngeal, verbal column, and thoracic

9.2 Planes of the Body

Table 12: Planes of Body (*Anatomical Terminology*, n.d.)

Axis	Description	Image
Coronal/Frontal Plane	Vertical plane splitting the body into anterior and posterior and running from side to side	
Sagittal/Lateral Plane	Vertical plane dividing the body into left and right sides, runs from the front to the back	
Axial/Transverse Plane	Horizontal plane, divides body into upper and lower parts	
Median Plane	Sagittal plane that goes through the midline of the body, dividing the body and its parts into left and right halves	

9.3 Ligament Function and Anatomy

Table 13: Glenohumeral ligaments Function and Anatomy (Dekker, 2020).

Ligament	Function	Anatomical Information
Superior	<ul style="list-style-type: none"> ● Important stabilizer of the adducted shoulder, limit external rotation of the abducted arm restraints up to 50 degrees abduction and external rotation ● Limits external rotation and inferior translation of humeral head 	<ul style="list-style-type: none"> ● Goes from glenoid and inserts onto the anatomical neck of humerus ● Bony footprint on glenoid neck
Middle	<ul style="list-style-type: none"> ● Becomes taut at 45 degree abduction, contributes to anterior stability, carried loading at 30, 60, and 90 degree abduction ● Limits external rotation, superior and anterior humeral head translation ● Limits internal rotation and anterior translation 	<ul style="list-style-type: none"> ● Goes from glenoid and inserts on humerus beyond lesser tuberosity
Inferior (including Anteroinferior and Posteroinferior)	<ul style="list-style-type: none"> ● Anterior band of inferior GL external rotation and restrain anterior and inferior translation of humerus , primary stabilize at 0 abduction 	<ul style="list-style-type: none"> ● Anterior band of inferior GL originates from anterior labrum and attaches to glenoid through collagen fibers attached at acute angle and fibers run parallel to surface and blend with periosteum ● Anterior band of inferior GL Humeral insertion on the inferior margin of articular surface of anatomic neck below tuberosity (collarlike insertion on the entire complex to articulate edge and v-shape attachment with anterior and posterior bands attaching to the articular cartilage)

Table 14: Ligament function and Anatomy (Dekker, 2020).

Ligament	Function	Anatomical Information
Coracohumeral	<ul style="list-style-type: none"> ● important inferior stability and limits external rotation of that a ducted arm (anterior band restraints up to 50 degree abduction and external rotation) (posterior elongated with internal rotation) ● Split into anterior and posterior by biceps, anterior limits extension, posterior limits flexion, both limit inferior and posterior translations of humeral head ● Supports weight of resting arm 	<ul style="list-style-type: none"> ● Originates from dorsolateral base of coracoid process, extends two bands to greater tuberosity and to lesser tuberosity (some of the ligament form a tunnel for the biceps on the anterior side of joint, also blends with superior Glenohumeral ligament) ● From coracoid process to humerus (covers SGHL and blends with superior joint capsule and supraspinatus tendon superiority)
Coracoacromial (CAL)	<ul style="list-style-type: none"> ● Prevents translation of humeral head 	<ul style="list-style-type: none"> ● Connects acromion and concord process on the scapula
Acromioclavicular (AC)		<ul style="list-style-type: none"> ● Connects acromion of scapula to lateral end of clavicle
Coracoclavicular (CC)		<ul style="list-style-type: none"> ● Connect clavicle to acromion of scapula

9.4 Materials Considered

The materials we considered for muscles, tendons, and ligaments were PLA, Nylon, TPU, Objet Tango Black, Formlabs Flexible, Formlabs Elastic, Moldstar 30 Silicone Rubber, and rubber exercise bands. The design criteria that we evaluated these materials based on included biological accuracy, resistance to plastic deformation, manufacturability, time to manufacture, and cost. Biological accuracy and resistance to plastic deformation were the most important criteria, which is reflected in our weighting. We scored each material on a scale of 1-5 for each criteria. The design matrix with total weighted scores as well as an explanation of scoring is shown below:

Table 15: Design Matrix for Weighing Material Selection Options

Design Criteria	Weight	PLA	Nylon	TPU	Objet Tango Black	Formlabs Flexible	Formlabs Elastic	Moldstar 30 Silicone Rubber	Latex Exercise Bands
Cost	10.00%	5	4	4	1	3	3	4	5
Resistance to Plastic Deformation	35.00%	5	5	5	5	5	5	4	5
Biological Accuracy	35.00%	1	1	3	3	4	4	2	4
Manufacturability	10.00%	5	5	5	3	4	4	4	4
Time to manufacture	10.00%	5	5	5	1	5	5	3	5
	100.00%	3.6000	3.5000	4.2000	3.3000	4.3500	4.3500	3.2000	4.400

Table 16: Explanation of Criteria Scoring for Materials

	1	3	5
Cost	High cost, will go over budget	Moderate cost, would use some of budget but not all	Very low or no cost
Resistance to Plastic Deformation	Would deform with single use of model	May have plastic deformation after many cycles	No Deformation
Closeness to natural material property	None of the properties are within the same order of magnitude as the biological material	Material matches within the same order of magnitude for most properties	Material properties are identical to natural material
Manufacturability	Outsource Everything	Some onsite, some offsite	Everything is onsite and easily accessible
Time to Manufacture	Would take 4 weeks or more to make	Would take 2-3 weeks	Would take 1 week or less to make

Based on this scoring, we found that TPU, Formlabs Elastic, and Formlabs Flexible are our most promising materials. These materials possess elastic moduli within the range of tendons and ligaments. These materials also have a high enough yield strength to withstand the forces present in the model without plastically deforming. Additionally, they are all cost effective and time efficient. The TPU, Formlabs Elastic, and Formlabs Flexible are also easy to manufacture, since they are all 3D printable using the printing labs available at WPI.

Although the Objet printer materials interested us, they were also the most expensive materials on our list, costing \$20-30 per cubic inch. We were concerned that the cost may be too high to fit within the budget, so we conducted some preliminary cost evaluations. Our preliminary calculations assumed that all of the muscles and tendons together would total approximately 20 cubic inches in volume. This would total between \$400 and \$600 in printing costs for our muscles and tendons, which was more than half of our budget. This cost would not include the price of printing dog-bone samples for material testing nor the cost of reprinting muscles if needed. Additionally, if the printer needed to be purged, that would add a minimum \$20 fee to the printing costs. In addition to the fee, purging the printer would also add several

days to the printing time of the objects. We encountered this issue the first time we attempted to print with the Objet printer and we were concerned that if this instance occurred throughout the project it would affect our ability to print all of the tendons and muscles in a timely manner.

We also decided to not move forward with the PLA and nylon because preliminary research into their material properties indicated they had modulus of elasticity and ultimate stresses that greatly exceeded that of biological muscles, tendons, and ligaments. We decided to not pursue the Moldstar 30 silicone rubber because of manufacturing concerns of the molding process which could take a long time and waste materials. After printing some Formlabs Flexible to be used as a ligament sleeve, we found that the material was not pliable enough to work for our ligaments so we evaluated our material choices and looked for a better material. We found that rubber exercise bands also scored highly in the decision matrix and were easier to manipulate and work with.

9.5 Attachment Methods Considered

In order to determine which attachment method to move forward with, we used a decision matrix for both the Bone to Tendon and Tendon to Muscle attachments. We evaluated the attachment methods by scoring the attachments by the design criteria on a scale of one to five and created a weighted total score for each attachment method. These are shown in the decision matrices below.

Table 17: Decision Matrix for Attachment Methods

Design Criteria	Weight	Bone to Tendon Attachment Methods			Tendon to Muscle Attachment Methods				
		Weld PLA and TPU	Screws	Adhesives	Nut and Bolt	Objet Material Gradient	Sewing	Suturing	KT Tape*
Manufacturability	13.33%	5	5	5	5	4	5	5	5
Bio-mechanical Accuracy	33.33%	3	3	4	2	4	3	5	2
Durability	26.67%	5	5	3	3	4	2	4	1
Time	13.33%	5	5	3	5	1	5	4	5
Cost	10.00%	5	5	5	5	1	5	4	5
Maintenance	3.33%	5	5	3	3	5	3	4	1
TOTAL	1	4.33333	4.33333	3.80000	3.40000	3.33333	3.46667	4.46667	2.80000

*Note that KT tape is also used to replicate the AC ligament in the model. KT Tape was evaluated for its feasibility as a tendon to muscle attachment in this table.

Table 18: Explanation of Scoring for Attachments

	1	3	5
Manufacturability	Outsource Everything	Some onsite, some offsite	Everything is onsite and easily accessible
Biomechanical Accuracy	None	Able to replicate some similar features to the human body	Extremely life-like
Durability	Deforms or breaks immediately when pulled by hand	Withstands some force, but eventually deforms or breaks when pulled by hand	Unable to break when pulling by hand
Time	Would take 4 weeks or more to complete	Take around 2-3 weeks to complete	1 week or less to complete
Cost	Not feasible with the given budget	Some cost but would fit within the budget	Little to no cost
Maintenance	Requires maintenance after each use	Average/Typical amount of maintenance	Requires very little or no maintenance

Based on these final scores, we found that welding and screws were equally good attachment methods for tendon to bone attachment, due to being durable, easily manufactured, cost effective, and time efficient. However, we decided to not move forward with welding as an attachment method for bone to tendon due to its permanency. If we were to melt the TPU and PLA together it would be very difficult to adjust the attachment point or replace the material without leaving the PLA and TPU deformed or damaged. This would result in the bones and tendons likely needing to be reprinted if future teams need to modify the model. Therefore, we decided to pursue screws as an attachment method, since they are a more easily removable and adjustable attachment method.

In terms of tendon to muscle attachment, we determined that suturing would be the best attachment method. In addition to being easy to manufacture, durable, low cost, and time efficient, sutures would also be more biologically accurate, since they are an attachment method often used in surgeries on the human body. The nut-and-bolt method and sewing were also shown to be good attachment methods through our decision matrix. The main disadvantage of the nut-and-bolt method, however, is that it would have very low biomechanical accuracy. It also could create a large stress concentration in the muscles, which may cause the soft tissue material

to tear. Sewing would be similar to suturing, however the main disadvantage is that it would be less durable and less biomechanically accurate compared to sutures.

9.6 Muscle Distances

Table 19: Distance of Muscles and motor movement

0-15 Degrees

Muscle	Motor	Type	StepsPerRev	Spool Dia. (mm)	Distance Per Step	TotalDistance (mm)	DistInSteps
SUP	1	Big	5400	25.4	0.0148	9.8	663
DLT	2	Big	5400	25.4	0.0148	18.5	1251
SA	3	Big	5400	25.4	0.0148	0	0
UT	4	Big	5400	25.4	0.0148	0	0
LT	5	Small	5400	25.4	0.0148	0	0

15-30 Degrees

Muscle	Motor	Type	StepsPerRev	Spool Dia. (mm)	Distance Per Step	TotalDistance (mm)	DistInSteps
SUP	1	Big	5400	25.4	0.0148	0	0
DLT	2	Big	5400	25.4	0.0148	13.6	920.34
SA	3	Big	5400	25.4	0.0148	0	0
UT	4	Big	5400	25.4	0.0148	0	0
LT	5	Small	5400	25.4	0.0148	0	0

30-60 Degrees

Muscle	Motor	Type	StepsPerRev	Spool Dia. (mm)	Distance Per Step	TotalDistance (mm)	DistInSteps
SUP	1	Big	5400	25.4	0.0148	21.4	1448.18
DLT	2	Big	5400	25.4	0.0148	30.6	2070.77
SA	3	Big	5400	25.4	0.0148	15.4	1042.15
UT	4	Big	5400	25.4	0.0148	20	1353.44
LT	5	Small	5400	25.4	0.0148	22	1488.79

60-90 Degrees

Muscle	Motor	Type	StepsPerRev	Spool Dia. (mm)	Distance Per Step	TotalDistance (mm)	DistInSteps
SUP	1	Big	5400	25.4	0.0148	0	0
DLT	2	Big	5400	25.4	0.0148	4.8	324.83
SA	3	Big	5400	25.4	0.0148	15.4	1042.15
UT	4	Big	5400	25.4	0.0148	20.1	1360.21
LT	5	Small	5400	25.4	0.0148	-22	-1488.79

9.7 Motor Code

The modified code from the previous team is shown below:

```
/*  
*/  
  
#include <AccelStepper.h>  
#include <MultiStepper.h>  
#include <SoftwareSerial.h>  
  
//Input each muscle motor  
AccelStepper SUP(1,7,6); //Supraspinatus Motor  
AccelStepper DLT(1,11,10); //Deltoid Motor  
AccelStepper SA(1,5,4); //Serratus Anterior Motor  
AccelStepper UT(1,9,8); //Upper Trapezius Motor  
AccelStepper LT(1,3,2); //Lower Trapezius Motor  
MultiStepper steppers; //On object to call all motors  
  
void setup() {  
  Serial.begin(9600); //Starts serial monitor  
  stepperSpeeds(500,500,500,500,500); // Sets the maximum stepper  
  speeds (SUP, DLT, SA, UT, LT)  
  steppers.addStepper(SUP); //add SUP motor to multistepper "stepper"  
  object  
  steppers.addStepper(DLT); //add DLT motor to multistepper "stepper"  
  object  
  steppers.addStepper(SA); //add SA motor to multistepper "stepper" object  
  steppers.addStepper(UT); //add UT motor to multistepper "stepper" object  
  steppers.addStepper(LT); //add LT motor to multistepper "stepper" object  
}
```

```

//create move function to move all motors at once
void makeMove(int posSUP, int posDLT, int posSA, int posUT, int posLT){
    long pos[5]= {0,0,0,0}; // Array of desired stepper positions, put motor
    positions in stepper speed function
    pos[0] = posSUP; //SUP pos
    pos[1] = posDLT; //DLT pos
    pos[2] = posSA; //SA pos
    pos[3] = posUT; //UT pos
    pos[4] = posLT; //LT pos
    steppers.moveTo(pos); //moves all steppers to assigned positions
    steppers.runSpeedToPosition(); // this is a blocking function, and does
not continue code until complete
}

//Set speed of all motors with one functions
void stepperSpeeds(int speedSUP, int speedDLT, int speedSA, int speedUT,
int speedLT){
    long pos[5]; // Array of desired stepper speeds, put motor speeds in
    stepper Speed function
    pos[0] = speedSUP;
    pos[1] = speedDLT;
    pos[2] = speedSA;
    pos[3] = speedUT;
    pos[4] = speedLT;
    SUP.setMaxSpeed(speedSUP); //SUP Speed
    DLT.setMaxSpeed(speedDLT); //DLT speed
    SA.setMaxSpeed(speedSA); //SA speed
    UT.setMaxSpeed(speedUT); //UT speed
    LT.setMaxSpeed(speedLT); //LT speed
}

void printAll(void){
    Serial.print("currPosition");
    Serial.println(SUP.currentPosition());
    Serial.println(DLT.currentPosition());
    Serial.println(SA.currentPosition());
    Serial.println(UT.currentPosition());
    Serial.println(LT.currentPosition());
}

```

```
//Movement of motors
void loop(){
  printAll();
  delay(7000);

  stepperSpeeds(100,313,0,0,0);    /// Change maximum stepper
  speeds(SUP,DLT,SA,UT,LT)
  makeMove(663, -1251, 0, 0, 0); //Move 0-15 degrees
  Serial.print("0-15 degrees");
  printAll();

  stepperSpeeds(0,230,0,0,0); // Change maximum stepper
  speeds(SUP,DLT,SA,UT,LT)
  makeMove(663, -2172, 0, 0, 0); //Move 15-30 degrees
  Serial.print("15-30 degrees");
  printAll();

  stepperSpeeds(300,586,240,339,390); // Change maximum stepper
  speeds(SUP,DLT,SA,UT,LT)
  makeMove(2111, -4919, 1921, 2706, 3113); //Move 30-60 degrees
  Serial.print("30-60 degrees");
  printAll();

  stepperSpeeds(300,100,240,171,390); // Change maximum stepper
  speeds(SUP,DLT,SA,UT,LT)
  makeMove(2111, -5300, -1921, 4067, 0); //Move 60-90 degrees
  Serial.print("60-90 degrees");
  printAll();

  delay(2000); //delay before abduction

  stepperSpeeds(300,586,240,339,390); // // Change maximum stepper
  speeds(SUP,DLT,SA,UT,LT)
  makeMove(2111, -4919, 1921, 2706, 3113); //Move 90-60 degrees
  Serial.print("90-60 degrees");
  printAll();
```

```
stepperSpeeds(300,230,500,500,500); // Change maximum stepper
speeds(SUP,DLT,SA,UT,LT)
makeMove(663, -2172, 0, 0, 0); //Move 60-30 degrees
Serial.print("60-30 degrees");
printAll();

stepperSpeeds(100,313,500,500,500); // Change maximum stepper
speeds(SUP,DLT,SA,UT,LT)
makeMove(663, -1251, 0, 0, 0); //Move 30-15 degrees
Serial.print("30-15 degrees");
printAll();

stepperSpeeds(100,313,500,500,500); // Change maximum stepper
speeds(SUP,DLT,SA,UT,LT)
makeMove(0, 0, 0, 0, 0); //move 15-0 degrees
Serial.print("15-0 degrees");
printAll();

delay(5000);
}
```


9.8 ATSM Standard Used



pieces of abrasive cloth, abrasive paper, or plastic, or rubber-coated fabric, commonly called hospital sheeting, between the specimen and the grip surface. No. 80 double-sided abrasive paper has been found effective in many cases. An open-mesh fabric, in which the threads are coated with abrasive, has also been effective. Reducing the cross-sectional area of the specimen may also be effective. The use of special types of grips is sometimes necessary to eliminate slippage and breakage in the grips.

5.1.4 Drive Mechanism—A drive mechanism for imparting a uniform, controlled velocity to the movable member with respect to the stationary member. This velocity is to be regulated as specified in Section 8.

5.1.5 Load Indicator—A suitable load-indicating mechanism capable of showing the total tensile load carried by the test specimen when held by the grips. This mechanism shall be essentially free of inertia lag at the specified rate of testing and shall indicate the load with an accuracy of $\pm 1\%$ of the indicated value, or better. The accuracy of the testing machine shall be verified in accordance with Practices E4.

NOTE 6—Experience has shown that many testing machines now in use are incapable of maintaining accuracy for as long as the periods between inspection recommended in Practices E4. Hence, it is recommended that each machine be studied individually and verified as often as may be found necessary. It frequently will be necessary to perform this function daily.

5.1.6 The fixed member, movable member, drive mechanism, and grips shall be constructed of such materials and in such proportions that the total elastic longitudinal strain of the system constituted by these parts does not exceed 1% of the total longitudinal strain between the two gage marks on the test specimen at any time during the test and at any load up to the rated capacity of the machine.

5.1.7 Crosshead Extension Indicator—A suitable extension indicating mechanism capable of showing the amount of change in the separation of the grips, that is, crosshead movement. This mechanism shall be essentially free of inertial lag at the specified rate of testing and shall indicate the crosshead movement with an accuracy of $\pm 10\%$ of the indicated value.

5.2 Extension Indicator (extensometer)—A suitable instrument shall be used for determining the distance between two designated points within the gauge length of the test specimen as the specimen is stretched. For referee purposes, the extensometer must be set at the full gage length of the specimen, as shown in Fig. 1. It is desirable, but not essential, that this instrument automatically record this distance, or any change in it, as a function of the load on the test specimen or of the elapsed time from the start of the test, or both. If only the latter is obtained, load-time data must also be taken. This instrument shall be essentially free of inertia at the specified speed of testing. Extensometers shall be classified, and their calibration periodically verified in accordance with Practice E83.

5.2.1 Modulus-of-Elasticity Measurements—For modulus-of-elasticity measurements, an extensometer with a maximum strain error of 0.0002 mm/mm (in./in.) that automatically and continuously records shall be used. An extensometer classified by Practice E83 as fulfilling the requirements of a B-2

classification within the range of use for modulus measurements meets this requirement.

5.2.2 Low-Extension Measurements—For elongation-at-yield and low-extension measurements (nominally 20% or less), the same above extensometer, attenuated to 20% extension, is acceptable. In any case, the extensometer system must meet at least Class C (Practice E83) requirements, which include a fixed strain error of 0.001 strain or $\pm 1.0\%$ of the indicated strain, whichever is greater.

5.2.3 High-Extension Measurements—For making measurements at elongations greater than 20%, measuring techniques with error no greater than $\pm 10\%$ of the measured value are acceptable.

5.3 Micrometers—Apparatus for measuring the width and thickness of the test specimen shall comply with the requirements of Test Method D5947.

6. Test Specimens

6.1 Sheet, Plate, and Molded Plastics:

6.1.1 Rigid and Semirigid Plastics—The test specimen shall conform to the dimensions shown in Fig. 1. The Type I specimen is the preferred specimen and shall be used where sufficient material having a thickness of 7 mm (0.28 in.) or less is available. The Type II specimen is recommended when a material does not break in the narrow section with the preferred Type I specimen. The Type V specimen shall be used where only limited material having a thickness of 4 mm (0.16 in.) or less is available for evaluation, or where a large number of specimens are to be exposed in a limited space (thermal and environmental stability tests, etc.). The Type IV specimen is generally used when direct comparisons are required between materials in different rigidity cases (that is, nonrigid and semirigid). The Type III specimen must be used for all materials with a thickness of greater than 7 mm (0.28 in.) but not more than 14 mm (0.55 in.).

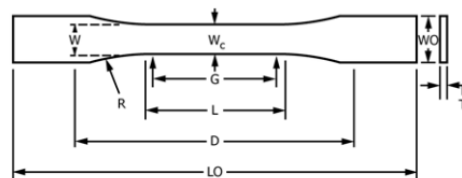
6.1.2 Nonrigid Plastics—The test specimen shall conform to the dimensions shown in Fig. 1. The Type IV specimen shall be used for testing nonrigid plastics with a thickness of 4 mm (0.16 in.) or less. The Type III specimen must be used for all materials with a thickness greater than 7 mm (0.28 in.) but not more than 14 mm (0.55 in.).

6.1.3 Reinforced Composites—The test specimen for reinforced composites, including highly orthotropic laminates, shall conform to the dimensions of the Type I specimen shown in Fig. 1.

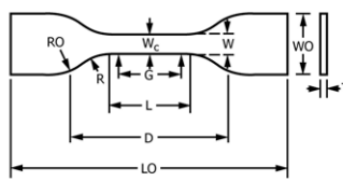
6.1.4 Preparation—Methods of preparing test specimens include injection molding, machining operations, or die cutting, from materials in sheet, plate, slab, or similar form. Materials thicker than 14 mm (0.55 in.) shall be machined to 14 mm (0.55 in.) for use as Type III specimens.

NOTE 7—Test results have shown that for some materials such as glass cloth, SMC, and BMC laminates, other specimen types should be considered to ensure breakage within the gage length of the specimen, as mandated by 7.3.

NOTE 8—When preparing specimens from certain composite laminates such as woven roving, or glass cloth, exercise care in cutting the specimens parallel to the reinforcement. The reinforcement will be significantly weakened by cutting on a bias, resulting in lower laminate properties, unless testing of specimens in a direction other than parallel


D638 – 22


TYPES I, II, III & V



TYPE IV

Specimen Dimensions for Thickness, T , mm (in.)^A

Dimensions (see drawings)	7 (0.28) or under		Over 7 to 14 (0.28 to 0.55), incl	4 (0.16) or under		Tolerances
	Type I	Type II	Type III	Type IV ^B	Type V ^{C,D}	
W —Width of narrow section ^{E,F}	13 (0.50)	6 (0.25)	19 (0.75)	6 (0.25)	3.18 (0.125)	± 0.5 (± 0.02) ^{B,C}
L —Length of narrow section	57 (2.25)	57 (2.25)	57 (2.25)	33 (1.30)	9.53 (0.375)	± 0.5 (± 0.02) ^C
WO —Width overall, min ^G	19 (0.75)	19 (0.75)	29 (1.13)	19 (0.75)	...	+ 6.4 (+ 0.25)
WO —Width overall, min ^G	9.53 (0.375)	+ 3.18 (+ 0.125)
LO —Length overall, min ^H	165 (6.5)	183 (7.2)	246 (9.7)	115 (4.5)	63.5 (2.5)	no max (no max)
G —Gage length ^I	50 (2.00)	50 (2.00)	50 (2.00)	...	7.62 (0.300)	± 0.25 (± 0.010) ^C
G —Gage length ^I	25 (1.00)	...	± 0.13 (± 0.005)
D —Distance between grips	115 (4.5)	135 (5.3)	115 (4.5)	65 (2.5) ^J	25.4 (1.0)	± 5 (± 0.2)
R —Radius of fillet	76 (3.00)	76 (3.00)	76 (3.00)	14 (0.56)	12.7 (0.5)	± 1 (± 0.04) ^C
RO —Outer radius (Type IV)	25 (1.00)	...	± 1 (± 0.04)

^AThickness, T , shall be 3.2 ± 0.4 mm (0.13 ± 0.02 in.) for all types of molded specimens, and for other Types I and II specimens where possible. If specimens are machined from sheets or plates, thickness, T , shall be the thickness of the sheet or plate provided this does not exceed the range stated for the intended specimen type. For sheets of nominal thickness greater than 14 mm (0.55 in.) the specimens shall be machined to 14 ± 0.4 mm (0.55 ± 0.02 in.) in thickness, for use with the Type III specimen. For sheets of nominal thickness between 14 and 51 mm (0.55 and 2 in.) approximately equal amounts shall be machined from each surface. For thicker sheets both surfaces of the specimen shall be machined, and the location of the specimen with reference to the original thickness of the sheet shall be noted. Tolerances on thickness less than 14 mm (0.55 in.) shall be those standard for the grade of material tested.

^BFor the Type IV specimen, the internal width of the narrow section of the die shall be 6.00 ± 0.05 mm (0.250 ± 0.002 in.). The dimensions are essentially those of Die C in Test Methods D412.

^CThe Type V specimen shall be machined or die cut to the dimensions shown, or molded in a mold whose cavity has these dimensions. The dimensions shall be:

$W = 3.18 \pm 0.03$ mm (0.125 ± 0.001 in.),

$L = 9.53 \pm 0.08$ mm (0.375 ± 0.003 in.),

$G = 7.62 \pm 0.02$ mm (0.300 ± 0.001 in.), and

$R = 12.7 \pm 0.08$ mm (0.500 ± 0.003 in.).

The other tolerances are those in the table.

^DSupporting data on the introduction of the L specimen of Test Method D1822 as the Type V specimen are available from ASTM Headquarters. Request RR:D20-1038.

^EThe tolerances of the width at the center W_c shall be $+0.00$ mm, -0.10 mm ($+0.000$ in., -0.004 in.) compared with width W at other parts of the reduced section. Any reduction in W at the center shall be gradual, equally on each side so that no abrupt changes in dimension result.

^FFor molded specimens, a draft of not over 0.13 mm (0.005 in.) is allowed for either Type I or II specimens 3.2 mm (0.13 in.) in thickness. See diagram below and this shall be taken into account when calculating width of the specimen. Thus a typical section of a molded Type I specimen, having the maximum allowable draft, could be as follows:

^GOverall widths greater than the minimum indicated are used for some materials in order to avoid breaking in the grips.

^HOverall lengths greater than the minimum indicated are used for some materials to avoid breaking in the grips or to satisfy special test requirements.

^ITest marks or initial extensometer span.

^JWhen self-tightening grips are used, for highly extensible polymers, the distance between grips will depend upon the types of grips used and may not be critical if maintained uniform once chosen.

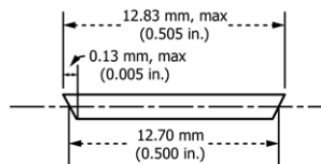
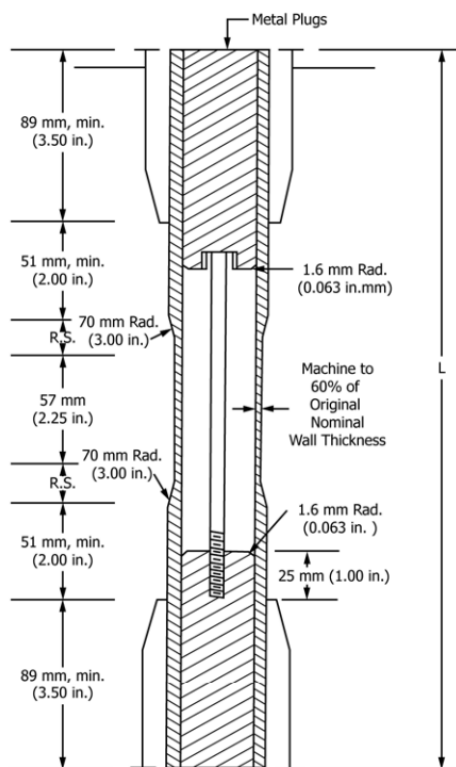


FIG. 1 Tension Test Specimens for Sheet, Plate, and Molded Plastics


D638 – 22


DIMENSIONS OF TUBE SPECIMENS

Nominal Wall Thickness	Length of Radial Sections, 2R.S.	Total Calculated Minimum Length of Specimen	Standard Length, L, of Specimen to Be Used for 89-mm (3.5-in.) Jaws ⁴
mm (in.)			
0.79 (1/32)	13.9 (0.547)	350 (13.80)	381 (15)
1.2 (3/64)	17.0 (0.670)	354 (13.92)	381 (15)
1.6 (1/16)	19.6 (0.773)	356 (14.02)	381 (15)
2.4 (3/32)	24.0 (0.946)	361 (14.20)	381 (15)
3.2 (1/8)	27.7 (1.091)	364 (14.34)	381 (15)
4.8 (3/16)	33.9 (1.333)	370 (14.58)	381 (15)
6.4 (1/4)	39.0 (1.536)	376 (14.79)	400 (15.75)
7.9 (5/16)	43.5 (1.714)	380 (14.96)	400 (15.75)
9.5 (3/8)	47.6 (1.873)	384 (15.12)	400 (15.75)
11.1 (7/16)	51.3 (2.019)	388 (15.27)	400 (15.75)
12.7 (1/2)	54.7 (2.154)	391 (15.40)	419 (16.5)

⁴For jaws greater than 89 mm (3.5 in.), the standard length shall be increased by twice the length of the jaws minus 178 mm (7 in.). The standard length permits a slippage of approximately 6.4 to 12.7 mm (0.25 to 0.50 in.) in each jaw while maintaining the maximum length of the jaw grip.

FIG. 2 Diagram Showing Location of Tube Tension Test Specimens in Testing Machine

with the reinforcement constitutes a variable being studied.

NOTE 9—Specimens prepared by injection molding may have different tensile properties than specimens prepared by machining or die-cutting because of the orientation induced. This effect may be more pronounced in specimens with narrow sections.

6.2 *Rigid Tubes*—The test specimen for rigid tubes shall be as shown in Fig. 2. The length, L , shall be as shown in the table in Fig. 2. A groove shall be machined around the outside of the specimen at the center of its length so that the wall section after machining shall be 60 % of the original nominal wall thickness. This groove shall consist of a straight section 57.2 mm (2.25 in.) in length with a radius of 76 mm (3 in.) at each end joining it to the outside diameter. Steel or brass plugs having diameters such that they will fit snugly inside the tube and having a length equal to the full jaw length plus 25 mm (1 in.) shall be placed in the ends of the specimens to prevent crushing. They can be located conveniently in the tube by separating and supporting them on a threaded metal rod. Details of plugs and test assembly are shown in Fig. 2.

6.3 *Rigid Rods*—The test specimen for rigid rods shall be as shown in Fig. 3. The length, L , shall be as shown in the table in Fig. 3. A groove shall be machined around the specimen at the center of its length so that the diameter of the machined portion shall be 60 % of the original nominal diameter. This groove shall consist of a straight section 57.2 mm (2.25 in.) in length with a radius of 76 mm (3 in.) at each end joining it to the outside diameter.

6.4 All surfaces of the specimen shall be free of visible flaws, scratches, or imperfections. Marks left by coarse machining operations shall be carefully removed with a fine file or abrasive, and the filed surfaces shall then be smoothed with abrasive paper (No. 00 or finer). The finishing sanding strokes shall be made in a direction parallel to the long axis of the test specimen. All flash shall be removed from a molded specimen, taking great care not to disturb the molded surfaces. In machining a specimen, undercuts that would exceed the dimensional tolerances shown in Fig. 1 shall be scrupulously avoided. Care shall also be taken to avoid other common machining errors.

6.5 If it is necessary to place gage marks on the specimen, this shall be done with a wax crayon or India ink that will not affect the material being tested. Gage marks shall not be scratched, punched, or impressed on the specimen.


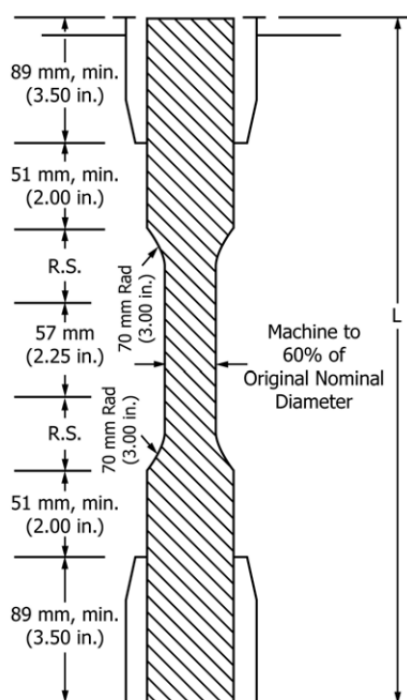
6.6 When testing materials that are suspected of anisotropy, duplicate sets of test specimens shall be prepared, having their long axes respectively parallel with, and normal to, the suspected direction of anisotropy.

7. Number of Test Specimens

7.1 Test at least five specimens for each sample in the case of isotropic materials.

7.2 For anisotropic materials, when applicable, test five specimens, normal to, and five parallel with, the principal axis of anisotropy.

7.3 Discard specimens that break at some flaw, or that break outside of the narrow cross-sectional test section (Fig. 1, dimension “ L ”), and make retests, unless such flaws constitute a variable to be studied.


D638 – 22

DIMENSIONS OF ROD SPECIMENS

Nominal Diameter	Length of Radial Sections, 2R.S.	Total Calculated Minimum Length of Specimen	Standard Length, <i>L</i> , of Specimen to Be Used for 89-mm (3.5-in.) Jaws ^A
mm (in.)			
3.2 (1/8)	19.6 (0.773)	356 (14.02)	381 (15)
4.7 (1/4)	24.0 (0.946)	361 (14.20)	381 (15)
6.4 (1/4)	27.7 (1.091)	364 (14.34)	381 (15)
9.5 (3/8)	33.9 (1.333)	370 (14.58)	381 (15)
12.7 (1/2)	39.0 (1.536)	376 (14.79)	400 (15.75)
15.9 (5/8)	43.5 (1.714)	380 (14.96)	400 (15.75)
19.0 (3/4)	47.6 (1.873)	384 (15.12)	400 (15.75)
22.2 (7/8)	51.5 (2.019)	388 (15.27)	400 (15.75)
25.4 (1)	54.7 (2.154)	391 (15.40)	419 (16.5)
31.8 (1 1/4)	60.9 (2.398)	398 (15.65)	419 (16.5)
38.1 (1 1/2)	66.4 (2.615)	403 (15.87)	419 (16.5)
42.5 (1 3/4)	71.4 (2.812)	408 (16.06)	419 (16.5)
50.8 (2)	76.0 (2.993)	412 (16.24)	432 (17)

^AFor jaws greater than 89 mm (3.5 in.), the standard length shall be increased by twice the length of the jaws minus 178 mm (7 in.). The standard length permits a slippage of approximately 6.4 to 12.7 mm (0.25 to 0.50 in.) in each jaw while maintaining the maximum length of the jaw grip.

FIG. 3 Diagram Showing Location of Rod Tension Test Specimen in Testing Machine

NOTE 10—Before testing, all transparent specimens should be inspected in a polariscope. Those which show atypical or concentrated strain patterns should be rejected, unless the effects of these residual strains constitute a variable to be studied.

8. Speed of Testing

8.1 Speed of testing shall be the relative rate of motion of the grips or test fixtures during the test. The rate of motion of the driven grip or fixture when the testing machine is running idle may be used, if it can be shown that the resulting speed of testing is within the limits of variation allowed.

8.2 Choose the speed of testing from **Table 1**. Determine this chosen speed of testing by the specification for the material being tested, or by agreement between those concerned. When the speed is not specified, use the lowest speed shown in **Table 1** for the specimen geometry being used, which gives rupture within 0.5 to 5-min testing time.

8.3 Make modulus determinations at the speed selected for the other tensile properties when the recorder response and resolution are adequate.

9. Conditioning

9.1 *Conditioning*—Condition the test specimens in accordance with Procedure A of Practice **D618**, unless otherwise specified by contract or the relevant ASTM material specification. Conditioning time is specified as a minimum. Temperature and humidity tolerances shall be in accordance with Section 7 of Practice **D618** unless specified differently by contract or material specification.

9.2 *Test Conditions*—Conduct the tests at the same temperature and humidity used for conditioning with tolerances in accordance with Section 7 of Practice **D618**, unless otherwise specified by contract or the relevant ASTM material specification.

10. Procedure

10.1 Measure the width and thickness of each specimen to the nearest 0.025 mm (0.001 in.) using the applicable test methods in **D5947**.

TABLE 1 Designations for Speed of Testing^A

Classification ^B	Specimen Type	Speed of Testing, mm/min (in./min)	Nominal Strain ^C Rate at Start of Test, mm/mm·min (in./in.·min)
Rigid and Semirigid	I, II, III rods and tubes	5 (0.2) ± 25 %	0.1
		50 (2) ± 10 %	1
	IV	500 (20) ± 10 %	10
		5 (0.2) ± 25 %	0.15
		50 (2) ± 10 %	1.5
		500 (20) ± 10 %	15
Nonrigid	V	1 (0.05) ± 25 %	0.1
		10 (0.5) ± 25 %	1
	III	100 (5) ± 25 %	10
		50 (2) ± 10 %	1
		500 (20) ± 10 %	10
		50 (2) ± 10 %	1.5
IV	50 (20) ± 10 %	15	

^ASelect the lowest speed that produces rupture in 0.5 to 5 min for the specimen geometry being used (see 8.2).

^BSee Terminology **D883** for definitions.

^CThe initial rate of straining cannot be calculated exactly for dumbbell-shaped specimens because of extension, both in the reduced section outside the gage length and in the fillets. This initial strain rate can be measured from the initial slope of the tensile strain-versus-time diagram.



10.1.1 Measure the width and thickness of flat specimens at the center of each specimen and within 5 mm of each end of the gage length.

10.1.2 For injection molded specimens, the actual measurement of only one specimen from each sample will suffice when it has previously been demonstrated that the specimen-to-specimen variation in width and thickness is less than 1 %.

10.1.3 For thin sheeting, including film less than 1.0 mm (0.04 in.), take the width of specimens produced by a Type IV die as the distance between the cutting edges of the die in the narrow section. For all other specimens, measure the actual width of the center portion of the specimen to be tested, unless it can be shown that the actual width of the specimen is the same as that of the die within the specimen dimension tolerances given in Fig. 1.

10.1.4 Measure the diameter of rod specimens, and the inside and outside diameters of tube specimens, to the nearest 0.025 mm (0.001 in.) at a minimum of two points 90° apart; make these measurements along the groove for specimens so constructed. Use plugs in testing tube specimens, as shown in Fig. 2.

10.2 Place the specimen in the grips of the testing machine, taking care to align the long axis of the specimen and the grips with an imaginary line joining the points of attachment of the grips to the machine. The distance between the ends of the gripping surfaces, when using flat specimens, shall be as indicated in Fig. 1. On tube and rod specimens, the location for the grips shall be as shown in Fig. 2 and Fig. 3. Tighten the grips evenly and firmly to the degree necessary to prevent slippage of the specimen during the test, but not to the point where the specimen would be crushed.

10.3 Attach the extension indicator. When modulus is being determined, a Class B-2 or better extensometer is required (see 5.2.1).

NOTE 11—Modulus of materials is determined from the slope of the linear portion of the stress-strain curve. For most plastics, this linear portion is very small, occurs very rapidly, and must be recorded automatically. The change in jaw separation is never to be used for calculating modulus or elongation.

10.4 Set the speed of testing at the proper rate as required in Section 8, and start the machine.

10.5 Record the load-extension curve of the specimen.

10.6 Record the load and extension at the yield point (if one exists) and the load and extension at the moment of rupture.

NOTE 12—If it is desired to measure both modulus and failure properties (yield or break, or both), it may be necessary, in the case of highly extensible materials, to run two independent tests. The high magnification extensometer normally used to determine properties up to the yield point may not be suitable for tests involving high extensibility. If allowed to remain attached to the specimen, the extensometer could be permanently damaged. A broad-range incremental extensometer or hand-rule technique may be needed when such materials are taken to rupture.

11. Calculation

11.1 Toe compensation shall be made in accordance with Annex A1, unless it can be shown that the toe region of the curve is not due to the take-up of slack, seating of the specimen, or other artifact, but rather is an authentic material response.

11.2 *Tensile Strength*—Calculate the tensile strength by dividing the maximum load sustained by the specimen in newtons (pounds-force) by the average original cross-sectional area in the gage length segment of the specimen in square metres (square inches). Express the result in pascals (pounds-force per square inch) and report it to three significant figures as tensile strength at yield or tensile strength at break, whichever term is applicable. When a nominal yield or break load less than the maximum is present and applicable, it is often desirable to also calculate, in a similar manner, the corresponding tensile stress at yield or tensile stress at break and report it to three significant figures (see Note A2.8).

11.3 Elongation values are valid and are reported in cases where uniformity of deformation within the specimen gage length is present. Elongation values are quantitatively relevant and appropriate for engineering design. When non-uniform deformation (such as necking) occurs within the specimen gage length nominal strain values are reported. Nominal strain values are of qualitative utility only.

11.3.1 *Percent Elongation*—Percent elongation is the change in gage length relative to the original specimen gage length, expressed as a percent. Percent elongation is calculated using the apparatus described in 5.2.

11.3.1.1 *Percent Elongation at Yield*—Calculate the percent elongation at yield by reading the extension (change in gage length) at the yield point. Divide that extension by the original gage length and multiply by 100.

11.3.1.2 *Percent Elongation at Break*—Calculate the percent elongation at break by reading the extension (change in gage length) at the point of specimen rupture. Divide that extension by the original gage length and multiply by 100.

11.3.2 *Nominal Strain*—Nominal strain is the change in grip separation relative to the original grip separation expressed as a percent. Nominal strain is calculated using the apparatus described in 5.1.7.

11.3.2.1 *Nominal strain at break*—Calculate the nominal strain at break by reading the extension (change in grip separation) at the point of rupture. Divide that extension by the original grip separation and multiply by 100.

11.4 *Modulus of Elasticity*—Calculate the modulus of elasticity by extending the initial linear portion of the load-extension curve and dividing the difference in stress corresponding to any segment of section on this straight line by the corresponding difference in strain. All elastic modulus values shall be computed using the average original cross-sectional area in the gage length segment of the specimen in the calculations. The result shall be expressed in pascals (pounds-force per square inch) and reported to three significant figures.

11.5 *Secant Modulus*—At a designated strain, this shall be calculated by dividing the corresponding stress (nominal) by the designated strain. Elastic modulus values are preferable and shall be calculated whenever possible. However, for materials where no proportionality is evident, the secant value shall be calculated. Draw the tangent as directed in A1.3 and Fig. A1.2, and mark off the designated strain from the yield point where the tangent line goes through zero stress. The stress to be used


D638 – 22

in the calculation is then determined by dividing the load-extension curve by the original average cross-sectional area of the specimen.

11.6 For each series of tests, calculate the arithmetic mean of all values obtained and report it as the “average value” for the particular property in question.

11.7 Calculate the standard deviation (estimated) as follows and report it to two significant figures:

$$s = \sqrt{(\sum X^2 - n\bar{X}^2)/(n-1)} \quad (1)$$

where:

- s = estimated standard deviation,
- X = value of single observation,
- n = number of observations, and
- \bar{X} = arithmetic mean of the set of observations.

11.8 See **Annex A1** for information on toe compensation.

11.9 See **Annex A3** for the determination of Poisson’s Ratio.

12. Report

12.1 Report the following information:

12.1.1 Complete identification of the material tested, including type, source, manufacturer’s code numbers, form, principal dimensions, previous history, etc.,

12.1.2 Method of preparing test specimens,

12.1.3 Type of test specimen and dimensions,

12.1.4 Conditioning procedure used,

12.1.5 Atmospheric conditions in test room,

12.1.6 Number of specimens tested; for anisotropic materials, the number of specimens tested and the direction in which they were tested,

12.1.7 Speed of testing,

12.1.8 Classification of extensometers used. A description of measuring technique and calculations employed instead of a minimum Class-C extensometer system,

12.1.9 Tensile strength at yield or break, average value, and standard deviation,

12.1.10 Tensile stress at yield or break, if applicable, average value, and standard deviation,

12.1.11 Percent elongation at yield, or break, or nominal strain at break, or all three, as applicable, average value, and standard deviation,

12.1.12 Modulus of elasticity or secant modulus, average value, and standard deviation,

12.1.13 If measured, Poisson’s ratio, average value, standard deviation, and statement of whether there was proportionality within the strain range,

12.1.14 Date of test, and

12.1.15 Revision date of Test Method D638.

TABLE 2 Modulus, 10⁹ psi, for Eight Laboratories, Five Materials

	Mean	S_r	S_R	I_r	I_R
Polypropylene	0.210	0.0089	0.071	0.025	0.201
Cellulose acetate butyrate	0.246	0.0179	0.035	0.051	0.144
Acrylic	0.481	0.0179	0.063	0.051	0.144
Glass-reinforced nylon	1.17	0.0537	0.217	0.152	0.614
Glass-reinforced polyester	1.39	0.0894	0.266	0.253	0.753

13. Precision and Bias⁵

13.1 *Precision*—The precision of this test method is based on two interlaboratory studies of ASTM D638, Standard Test Method for Tensile Properties of Plastics, conducted in 1984 and 1988, respectively. **Tables 2-4** are based on eight laboratories who tested five different materials using Type I specimens of a nominal 3.175 mm (0.125 in.) thickness. Every “test result” represents five individual determinations. Each laboratory was asked to submit two replicate test results, from a single operator, for each material. Practice **E691** was followed for the design and analysis of the data; the details are given in ASTM Research Report No. D20-1125.

13.1.1 **Tables 5-8** are based on ten laboratories who tested eight different materials. For each material, all samples were molded at one source, but the individual specimens were prepared at the laboratories that tested them. Every “test result” represents five individual determinations. Each laboratory was asked to submit three test results, from a single operator for each material. Data from some laboratories could not be used for various reasons, and this is noted in each table. Practice **E691** was followed for the design and analysis of the data; the details are given in ASTM Research Report No. D20-1170.

13.1.2 **Tables 9 and 10** are based on eight laboratories who tested three different materials. For each material, all samples were molded at one source, but the individual specimens were prepared at the laboratories that tested them. Every “test result” represents five individual determinations. Each laboratory was asked to submit three test results, from a single operator, for each material. Practice **E691** was followed for the design and analysis of the data; the details are given in ASTM Research Report No. D20-1170.

13.1.3 The precision of this test method is very dependent upon the uniformity of specimen preparation, standard practices for which are covered in other documents.

13.2 *Bias*—There are no recognized standards on which to base an estimate of bias for this test method.

13.3 **Warning**—The data in **Tables 2-10** shall not be rigorously applied to acceptance or rejection of material, as those data are specific to the interlaboratory study and are not necessarily representative of other lots, conditions, materials, or laboratories. Users of this test method shall apply the

⁵ Supporting data are available from ASTM Headquarters. Request RR:D20-1125 for the 1984 round robin and RR:D20-1170 for the 1988 round robin.

TABLE 3 Tensile Stress at Break, 10³ psi, for Eight Laboratories, Five Materials^A

	Mean	S_r	S_R	I_r	I_R
Polypropylene	2.97	1.54	1.65	4.37	4.66
Cellulose acetate butyrate	4.82	0.058	0.180	0.164	0.509
Acrylic	9.09	0.452	0.751	1.27	2.13
Glass-reinforced polyester	20.8	0.233	0.437	0.659	1.24
Glass-reinforced nylon	23.6	0.277	0.698	0.784	1.98

^ATensile strength and elongation at break values obtained for unreinforced propylene plastics generally are highly variable due to inconsistencies in necking or “drawing” of the center section of the test bar. Since tensile strength and elongation at yield are more reproducible and relate in most cases to the practical usefulness of a molded part, they are generally recommended for specification purposes.

Appendix 9.9 Motion Tracking Data

Trial 1				
time from start of cycle	Humerus Abduction	Humerus Deviation	Scapula Rotation (back)	Scapula Rotation (top)
0	0	2.7	0	0
0.83	2	1.8	0	-0.2
1.74	4	0.8	0	0.1
2.97	6.1	-0.8	0	-0.2
3.74	8	-1.8	0	-0.2
4.47	10.1	-2.7	0	-0.1
5.14	12	-3	0	-0.2
5.84	14	-3.8	0	0
6.54	16	-4.9	0	-0.6
7.14	18	-6.2	0	-0.2
7.81	20	-7.7	0.3	-0.2
8.71	22	-9.1	0.3	-0.4
9.48	24.1	-10.7	0.3	-0.5
10.24	26	-11.9	0.6	-0.7
11.08	28	-13.3	1.7	-1.2
12.04	30	-14.4	3.7	-2.8
13.01	32.1	-14.9	5.3	-3.8
14.08	34	-16.4	6.5	-4.5
15.15	36	-17.5	8.1	-4.8
16.11	38.1	-19.9	9.4	-5.3
17.12	40	-24	10.6	-5.7
18.15	42	-27	11.3	-6.1
18.58	42.8	-30.1	11.5	-6.5
18.88	43	-30.1	11.5	-6.6
19.12	43	-30.1	11.8	-6.2
25.19	43.1	-29.9	11.8	-6.1
25.76	43.2	-30	12.2	-6.2

27.16	43.5	-30	12.5	-6.4
28	43.5	-29.8	12.2	-6.8
29	43.2	-29.7	11.7	-6.9
30	42.9	-29.5	11.9	-7.5
31	42.8	-28.9	11.1	-7.8
32	41.7	-29.1	9.7	-9
33	41.4	-29.5	8.9	-9.7
34	41.3	-29.6	8.1	-10.7
35	41	-29.5	7.7	-11.7

Trial 2				
time from start of cycle	Humerus Abduction	Humerus Deviation	Scapula Rotation (back)	Scapula Rotation (top)
0	0	4.1	0	0
2.04	2	4.1	0	-0.5
3.71	4	3.5	0.3	-0.1
4.81	6	2.8	0.4	-0.5
5.57	8.2	2.1	0.4	-0.9
6.41	10	1.6	0.4	-0.1
7.17	12	0.3	0.4	-0.5
8.31	14	-2.3	0.4	-0.6
9.21	16	-4.2	0.4	-0.9
10.01	18	-5.6	0.4	-0.2
10.68	20	-7	1	-0.1
11.45	22	-7.1	2.6	-2
12.31	24	-7.5	4.2	-3.8
13.15	26	-7.4	5.6	-3.9
14.11	28.1	-7.7	7.2	-4
14.68	30	-7.6	7.6	-4

15.72	32	-7.8	8.9	-4
16.38	34.1	-8.7	9.5	-4.1
16.85	36.2	-10.9	9.5	-4.1
17.55	38	-12.5	9.6	-4.5
17.78	38.3	-13.6	9.6	-4.6
18.25	38.8	-14.1	10.2	-4.6
19	38.8	-14.5	9.8	-4.5
20	38.7	-14.2	9.8	-4.6
21	38.6	-14.2	9.8	-4.1
22	38.4	-14.1	10.1	-4.1
23	38.1	-14	9.9	-4.1
24	37.3	-13.3	10.6	-5
25	37.1	-13.5	10.5	-5
26	35.8	-12.7	10	-6.3
27	35.8	-12.3	10.1	-5.8
28	35.4	-12.3	9.5	-6.3
29	35.3	-12.5	9.8	-6.7
30	35.1	-12.7	9.6	-6.7
31	34.7	-12.7	8.6	-6.3
32	34.1	-12.7	7.6	-6.7
33	33.9	-12.9	7.3	-6.7
34	33.9	-13.3	7.3	-7.1
35	34	-13.7	7.3	-7.1

Trial 3				
time from start of cycle	Humerus Abduction	Humerus Deviation	Scapula Rotation (back)	Scapula Rotation (top)
0	0	3.1	0	0
1.57	2	2.2	0	-0.4

2.64	4	1.1	0	-0.4
3.64	6	0.5	0.3	-0.1
4.37	8	0	0	0
5.31	10	-0.4	0	-0.4
6.57	12.1	-1.1	0	0
7.94	14	-2.2	0.3	0
9.64	16	-4.3	0.6	0
10.28	18.1	-5.6	0.6	0
10.74	20.1	-6.3	1	0.5
11.48	22	-6.8	1.9	-0.9
12.41	24.1	-6.9	3.5	-1.3
13.18	26	-7.4	4.9	-2.2
13.91	28	-8.2	6.3	-1.9
14.65	30	-9	7.5	-2.7
15.55	32.2	-9.8	8.7	-4.1
16.35	34	-11.1	9.7	-4.3
16.95	36.1	-12.3	10.3	-4.3
17.78	38	-13.9	11.1	-4.8
18.32	40	-16.1	12.3	-4.8
18.62	40.7	-17.5	12.3	-5.3
19.55	40.8	-18.2	12.6	-5.2
20	40.7	-18.2	12.3	-5.3
21	40.8	-18.2	12.3	-5.7
22	40.8	-18.2	12.4	-5.3
23	40.4	-17.7	12.6	-5.6
24	39	-16.2	12.1	-5.7
25	37.8	-14.4	11.5	-5.2
26	36.8	-13.2	11.2	-5.7
27	36	-12.7	11	-5.7
28	35.2	-12.1	10.7	-5.7

29	34.2	-11.7	9.2	-5.7
30	33.7	-11.6	8.9	-5.3
31	33.3	-11.1	8.9	-5.7
32	32.7	-10.5	8.7	-5.7
33	32.4	-10.3	8.6	-6.3
34	32	-9.9	8.7	-6.7
35	31.6	-9.7	8.6	-7.5